# FINE AND HYPERFINE STRUCTURE STUDIES OF Lu, Ho AND Pr ATOMS USING LASER OPTOGALVANIC SPECTROSCOPY
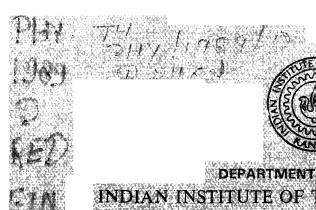
*by*

**MARTHA NARSI REDDY**

**DEPARTMENT OF PHYSICS**
**INDIAN INSTITUTE OF TECHNOLOGY, KANPUR**
FEBRUARY, 1989

# FINE AND HYPERFINE STRUCTURE STUDIES OF Lu, Ho AND Pr ATOMS USING LASER OPTOGALVANIC SPECTROSCOPY

A Thesis Submitted
In Partial Fulfilment of the Requirements
for the Degree of

## DOCTOR OF PHILOSOPHY

*by*

**MARTHA NARSI REDDY**

*to the*

**DEPARTMENT OF PHYSICS**

# INDIAN INSTITUTE OF TECHNOLOGY, KANPUR

**FEBRUARY, 1989**

PHY-1989 -D- RED - FIN

# CERTIFICATE

Certified that the work presented in  this  thesis  entitled "FINE AND HYPERFINE STRUCTURE STUDIES OF Lu, Ho AND Pr ATOMS USING LASER OPTOGALVANIC SPECTROSCOPY" has been carried  out by Mr.Martha Narsi Reddy under my supervision and  that  the same has not been submitted elsewhere for a degree.

Thesis Supervisor

February, 1989

(G.N.Rao)
Professor
Department of Physics
I.I.T. Kanpur

DEDICATED

TO

MY PARENTS

# ACKNOWLEDGEMENTS

## SYNOPSIS

## FINE AND HYPERFINE STRUCTURE STUDIES OF Lu, Ho AND Pr ATOMS USING LASER OPTOGALVANIC SPECTROSCOPY

MARTHA NARSI REDDY
Ph.D.
Department of physics
Indian Institute of Technology, Kanpur
January, 1989

The thesis deals with the experimental studies of the fine and the hyperfine structure of neutral atoms of some rare-earth elements. These studies were carried out using laser optogalvanic spectroscopy(LOGS) of sputtered atoms in hollow cathode dischages.

The thesis is organised in six chapters. Chapter I deals with an introduction to the subject "investigation of atomic and nuclear structure by means of optical spectroscopy". In this chapter, the objectives and the plan of the thesis are also briefly outlined.

Even though, the spectroscopic investigations of the rare-earth elements have been carried out for the past several decades, the knowledge about the atomic structure of these elements is far from complete. Rare-earth atoms with several electrons in the unclosed shells usually have a large number of electronic configurations. The interactions among these configurations are in general of the same order of magnitude and therefore it is very difficult to assign the coupling schemes to the electrons. Moreover, the rare-earth atoms consist of highly

deformed nuclei and from the nuclear point of view, it is of interest to determine the deformation parameters with the neutron number. The investigation of hyperfine structure of atomic states lead to valuable information regarding the basic properties of the atomic and the nuclear structure. The measurement of the hyperfine coupling constants enable us to find the electronic parameters like radial integrals and the nuclear parameters such as spins, and magnetic dipole and electric quadrupole moments.

The development of tunable dye lasers and a number of extremely sensitive and high resolution spectroscopic techniques during the past decade has resulted in a revolutionary advance in the spectroscopy of atoms and molecules. In this thesis laser optogalvanic spectroscopy was employed to study the fine and the hyperfine structure of many high-lying configurations of Lu,Ho and Pr.

Chapter II gives a brief review of the theory of the fine and the hyperfine structure of atoms. Elementary theory of the hyperfine structure of atoms and also the effective-operator formalism for the analysis of the hyperfine structure is briefly discussed.

Chapter III deals with the experimental details and the optogalvanic spectroscopy(OGS) technique. A simple phenomenological theory of the optogalvanic effect and the characteristics of the effect are briefly discussed. The change in the impedance of a gaseous discharge due to resonant absorption of light is a very sensitive effect and the corresponding optogalvanic signals are easily monitored without the need of an

optical detector. The production of sputtered atoms in the glow discharges of hollow cathode lamps and their potential applications for the study of spectroscopy are also discussed in this chapter.

The experimental arrangements for low resolution cw optogalvanic spectroscopy as well as for Doppler-limited high resolution OGS are described in section III.3. A brief description of the principles of dye laser operation and frequency stabilization and scanning procedures are given in section III.4. The OG spectra of neon, sodium and uranium are studied in the hollow cathode glow discharges as test cases for the calibration and optimization of the OG signals.The OG spectra of rubidium and cesium were also studied in the positive column of a glow discharge. The isotope shifts in the neon were measured using intermodulated optogalvanic spectroscopy (IMOGS) to test the frequency stability and resolution of the experimental set-up. Finally, the study of the OGS of neodimium using cw dye laser covering 5710-6400Å wavelength range is presented in section III.6. The observed relative intensities of all the identified transitions of NdI and NdII and the classification to many of the transitions are given.

Chapter IV is devoted to the experimental results obtained in lutetium using LOGS. The optogalvanic spectrum of lutetium was studied in the 5650-6250Å wavelength range and sixteen spectral lines of LuI were identified. Out of the identified sixteen lines, eight of them are reported for the first time. The classification for five of these new spectral lines of LuI is done using the

known energy levels of the high lying configurations $6s^2np$, $6s^2nd$, $5d6s7s$ and $6s^2nf$.

The hyperfine structure for many of the identified LuI transitions are studied for $^{175}$Lu isotope using LOGS with a single frequency dye laser as the excitation source. Most of the hfs components are well resolved even in the Doppler-limited hfs spectra which facilitated good computer fits and reliable analysis of the observed spectra. A short note of the fitting procedure and the error analysis is also presented in this chapter. The hyperfine coupling constants for eighteen energy levels of $^{175}$Lu are measured and the results are compared with the values available in the literature wherever applicable. The theoretically calculated hfs constants for 20432.53 cm$^{-1}$ and 22609.46cm$^{-1}$ states have been corrected using the present studies. The hfs constants for five levels of the three high lying configurations $5d6s7s$, $6s^27d$ and $6s^225p$ are reported for the first time.

Chapter V describes the experimental results on the fine and the hyperfine structure of many energy levels in holmium. The optogalvanic spectrum of holmium was recorded in 5650-6200Å wavelength range to detect several transitions of HoI between the excited metastable states and the multiplets of $4f^{11}6s7p$ and $4f^{11}6s7s$ highlying configurations. The observed relative intensities and classification to many of the observed spectral lines are presented.

The hyperfine structure spectra for twenty seven identified transitions of $^{165}$Ho are studied and the hyperfine coupling constants for the combining levels are calculated. The hfs

constants for nine of the high lying configurations are reported for the first time.

Chapter VI deals with the experimental results obtained on the fine and the hyperfine structure of praseodymium using LOGS. A highly dense atomic spectrum of praseodymium was recorded in 5700-6250Å wavelength range perhaps for the first time. From the large number of observed spectral lines, as many as 128 strong lines are identified either with PrI transitions or with PrII transitions. Out of these, thirty eight transitions of PrI are reported for the first time. The observed relative intensities and the classification for almost all the identified transitions of Pr are given in this chapter.

The hyperfine structure for sixteen transitions of PrI is studied and the hfs coupling constants for the corresponding levels were calculated. The hfs constants for eight high lying levels belonging to $4f^2 5d^2 6p$ and $4f^3 5d6p$ configurations are reported for the first time.

In conclusion, the merits and capabilities of LOGS for studying the highly excited energy levels of the rare-earth atoms are remarked. The importance of the study of the hyperfine structure of the rare-earth atoms to understand the high lying configurations which are often mixed is also discussed.

# T A B L E   O F   C O N T E N T S

# L I S T   O F   T A B L E S

# L I S T   O F   F I G U R E S

# CHAPTER I

## INTRODUCTION

Optical spectroscopy has been an important tool for the investigation of the atomic and the nuclear structure since the earliest days of atomic physics. The study of optical spectra of the simple hydrogen atom has played a central role in the development of atomic physics and quantum mechanics. The discovery of fine structure brought the concept of electron spin and the observation of hyperfine structure led to the realisation of magnetic and electric moments for the spinning nucleus.

With the discovery of a number of powerful spectroscopic techniques using lasers, the field of atomic spectroscopy has been totally revolutionized. The precision measurements of the fine structure of the atomic states have led to the development of relativistic quantum theory, the discovery of particle spins, the discovery of anamalous magnetic moment of the electron and the Lamb shift, and the development of modern quantum electrodynamics(QED). The measurement of nuclear spins and electric and magnetic multipole moments from optical hyperfine structure experiments have constituted much of the basis for the construction of nuclear models. The high precision spectroscopic measurements in many-electron atoms is of great interest now both in terms of better understanding of the quantum mechanics and refining the present theories of atomic structure. Rare-earth

elements which have many unpaired electrons in the valence shells are ideal candidates for the spectroscopic investigations of many interesting phenomena that occur in many-electron atoms. Investigations of the electron correlations, the coupling schemes, and the relativistic effects in these atoms are of great value for verifying the basic concepts used in the atomic structure theories.

The theoretical calculations of many-electron atomic structure commonly start from a central field approximation where it is assumed that the electrons move independently in the average field of the nucleus and the other electrons (Independent particle model). This field, in addition is assumed to be spherically symmetric. It is also usually assumed in these calculations that the nucleus is a point charge without structure. With this approximation it is possible to describe the general structure of atoms to a fair accuracy. However, to obtain the detailed structure of many-electron atoms, one has to have a much better approach than the central field approximation. For example, to describe the structure of many-electron atoms accurately, it is necessary to take into account not only the interaction of the electrons with the Coulomb field but also the mutual repulsion of the electrons. The strong interaction between electrons, mainly at small distances, implies that a single configuration is inadequate. Therefore, electron-correlation effects are explicitly taken into account via configuration-interaction (CI) methods. The fine structure interaction which results mainly due to the spin-orbit interaction requires complete relativistic treatment.

However, for lighter atoms the fine structure can be calculated quite accurately by using first-order non-relativistic perturbation theories. In heavy atoms this interaction becomes too large to be treated as a perturbation and therefore an exact analysis becomes necessary. Moreover in the fine structure interactions, it is assumed that the nucleus is a spherical point charge. But in reality, the nucleus is neither a point nor a spherical object. The nucleus is extended, and has structural features such as shape, angular momentum and distribution of charge and current. The residual interaction between the electrons in the atom and the nucleus is called hyperfine interaction, which is a perturbation to the fine structure energy levels of the atom. The hyperfine interaction is usually devided into two parts, one caused by the electromagnetic moments of the nucleus (hyperfine structure) and the other by the finite extension of the nucleus (isotope shift). Studies of hyperfine structure of the energy levels enable us to measure the nuclear spin, nuclear moments, and isotope shift. These quantities, in turn, provide vluable information about nuclear structure and the electron wave functions near the nucleus. The hyperfine structure for an atomic fine structure level arises due to the interaction between the open-shell atomic electrons and the static nuclear moments. The major contributions to this are from the magnetic dipole and the electric quadrupole interactions.

For heavy atoms the breakdown of the LS coupling and the relativistic effects are two important factors one has to consider in the hyperfine structure analysis. For lighter atoms LS coupling

is rather a good approximation, while for heavier atoms a gradual change towards the jj coupling limit takes place. Hence the wavefunctions are in general expanded as a linear combination of LS-coupled wavefunctions. The coefficients in the expansion are obtained from a least-squares fit of the theoretical term splittings to the observed splittings, keeping electrostatic integrals and spin-orbit constants as free parameters. Using an effective-operator formalism the relativistic effects and the effects of configuration interactions are treated more conveniently by means of LS-coupled wavefunctions. An analysis of the hyperfine structure spectrum of a trasition between two fine structure levels leads to the measurement of hyperfine coupling constants for the fine structure energy levels. These hyperfine structure constants are generally expressed in terms of hyperfine parameters which are interpreted as products of a nuclear moment and a radial hyperfine integral. With the help of known nuclear moments, it is possible to evaluate the experimental radial hyperfine integrals from the hyperfine parameters which may then be compared with the theoretical values in order to test the hyperfine structure theory. On the other hand, it is possible to calculate the nuclear moments from the experimental hyperfine parameters with the help of theoretically evaluated radial hyperfine integrals.

The availability of tunable dye lasers has greatly increased the power of atomic spectroscopy to contribute immensely to the knowledge of atomic and nuclear structure. Dye lasers with high spectral purity, high intensity,high degree of coherence,

polarization, tunability and low divergence are ideal light sources for high-resolution optical spectroscopy experiments. A variety of new experimental techniques with high resolution, high precision and high sensitivity have come into force mainly due to the infalliable instruments, the dye lasers. Combined with these new spectroscopic techniques the dye lasers have really enriched the field of hyperfine interactions.

In this thesis laser optogalvanic spectroscopic experiments on some rare-earth atoms are described. Investigation of the fine structure of neodymium, and the fine and the hyperfine structure of lutetium, holmium and praseodymium are carried out using the laser optogalvanic spectroscopic technique in hollow cathode discharge lamps. Doppler broadening of the rare-earth atoms at ambient temperature is often small compared to the large hyperfine splittings of the energy levels. Under these conditions, the Doppler-limited OGS technique can be employed quite effectively to study the hyperfine interactions in these atoms. The atomic spectroscopy of rare-earth atoms is still an active field because there are many interesting hidden phenomena which are yet to be understood. The rare-earth atoms with several electrons in an unclosed shell can have a large number of electronic configurations. In these configurations there exist many interactions which are of the same order of magnitude and therefore it is very difficult to evaluate the coupling scheme for the electrons. There is a special interest in the study of the hyperfine structure of many states of the configuration or an LS multiplet since they enable us to understand the different

contributions to the hyperfine structure in rare-earth atoms. The angular momenta of electrons in the unclosed 4f-shell of rare-earth elements are not purely LS coupled and it is suitable for the application of effective operator techniqués. Rare-earth atoms have highly deformed nuclei and therefore the determination of the deformation parameters with the neutron number for the rare-earth isotopes is of great interest to understand the systematics and trends in the variation of the nuclear properties of the isotopic chains of the nuclear chart.

Optogalvanic spectroscopy in hollow cathode discharges is a very convenient experimental method to study the atomic spectra of almost all the elements. In this method, the hollow cathode discharge lamp serves not only as a source of atoms, but also as a sensitive transducer for detecting the signals. In hollow cathode discharges the atoms of the cathode material are produced in the ground and the metastable states in high steady-state densities by sputtering process. These sputtered atoms rapidly lose their initial high kinetic energies by elastic collisions with rare gas atoms and become effectively thermalized. The high sensitivity and good signal-to-noise ratio of the optogalvanic technique make it a useful and convenient experimental method. Signals of the weak trasitions between the high-lying states can be quite efficiently detected. Inspite of the high density of the ions in the discharge and the associated collisions, LOGS can be used effectively for high resolution spectroscopic studies.

In chapter II, the general theory of the fine and the hyperfine structure is reviewed. The effective operator formalism

for the analysis of the hyperfine structure is briefly outlined.

The experimental details are presented in chapter III. A brief discussion of the optogalvanic spectroscopic technique and the salient features of it for high-resolution optical spectroscopy are also given. The basic principles of the ring dye laser and its performance are outlined. The experimental arrangements for the different studies undertaken in the present thesis are described. Optogalvanic spectra of neon, uranium and rubidium which were used for the purpose of calibration as well as optimization of the signals are given. The intermodulated optogalvanic spectra of neon provided a test case to check the frequency stability and resolution of the set-up.

Lastly, the optogalvanic spectra of neodymium recorded using cw dye laser is presented and the relative intensities of the observed spectra are tabulated.

The fine and the hyperfine structure studies of lutetium, holmium and praseodymium are presented in chapters IV, V, and VI respectively. In each case the optogalvanic spectra covering the rhodamin 6G dye range(with $Ar^+$ laser pumping) was studied. The relative intensities and the classification of the observed spectra are presented wherever possible. In the case of praseodymium the observed optogalvanic spectrum is very dense and contains a large number of spectral lines arising from many fine structure multiplets of both neutral and singly-ionised species. The hyperfine structure of several low as well as high-lying states in each case have been studied using Doppler-limited high resolution optogalvanic spectroscopy. Most of the hyperfine

components are well resolved in the observed hyperfine structure spectra of the elements studied. Various computer fits were carried out to analyse the hyperfine spectra to obtain the best values for the hyperfine coupling constants of the levels. The fitting procedures and the error analysis for the hyperfine structure spectra are discussed in chapter IV. In each case the hyperfine coupling constants for several levels of some high-lying configurations are reported for the first time. Hyperfine structure patterns of some unclassified spectral lines are also discussed.

CHAPTER I I

# THEORY OF FINE AND HYPERFINE STRUCTURE

## II.1 INTRODUCTION

The development of high resolving power spectroscopic instruments at the end of the nineteenth century led to the discovery of many finer details of the atomic structure. Michelson[1], Fabry and Perot [2], and Lummer and Gehrcke [3] noted that many atomic spectral lines consist of not only fine structure but, infact each fine structure line consisted of many closely spaced lines (hyperfine structure or hfs). In general, the hyperfine structure splitting for the atoms is of the order of $10-10^4$ MHz The fine structure of the atomic states is a relativistic phenomenon It arises due to the relativistic motion(orbital) of the electrons with intrinsic spins through the electric field caused by the nuclear charge[4]. The fine structure splitting is greater in the heavier elements and in general it is of the order of $10-10^3$ GHz. In 1924 Pauli[5] suggested that the hyperfine structure could be due to the interaction of the electrons in the atom with the magnetic moment of the nucleus. If this hypothesis is correct, the separation between the two adjacent hyperfine levels should follow the interval rule predicted by the magnetic dipole interaction. The deviation from this rule was first observed by Schuler and Schmidt[6] in the hfs of europium. Casimir[7] explained the experimental results

successfully by considering the electric quadrupole interaction with the nucleus in his theoretical calculations. Later, many accurate atomic-beam magnetic resonance (ABMR) experiments revealed the existence of the higher-order hyperfine interactions, such as the magnetic octupole and the electric hexadecapole interactions [8,9]. These higher-order hyperfine interactions are extremely weak and are about $10^8$ times smaller than the corresponding magnetic dipole and the electric qudrupole interactions. Schwartz[10] and Kopfermann[11] discussed the hyperfine structure theory of single electron atoms in great detail. Both relativistic and non-relativistic hyperfine structure theories of single electron and many electron atoms are reviewed recently by Armstrong[12] and Lindgren and Rosen[13].

## II.2   FINE STRUCTURE INTERACTION

In many-electron atoms, the fine structure is caused mainly due to the spin-orbit interaction. This is a magnetic interaction which results as the magnetic moment of the electron interacts with the magnetic field "seen" by the electron as it moves in the electrostatic field set up by the nuclear charge. The spin-orbit interaction splits the terms of a configuration into fine structure multiplets of closely spaced levels. There are a number of books[14,4] where the fine structure is described as a part of the general atomic structure. Here, the non-relativistic treatment of the general atomic structure is briefly reviewed.

Neglecting spin-orbit and hyperfine interactions, the Hamiltonian of an N-electron atom with nuclear charge Ze may be

written as

$$H = \sum_{i=1}^{N} \left( - \frac{\hbar^2}{2m} \nabla_i^2 - \frac{Ze^2}{4\pi\varepsilon_o r_i} \right) + \sum \frac{e^2}{4\pi\varepsilon_o r_{ij}} \qquad (2.1)$$

The first term in this expression represents the kinetic energy of the electrons, the second term, the coulomb attraction between the electrons and the nucleus and the last term the electrostatic repulsion between the electrons. In the mutual repulsion term the summation extends over all pairs of electrons. To determine the structure of an N-electron atom, one requires the solution of the Schrödinger equation

$$H \psi = E \psi \qquad (2.2)$$

The mutual repulsion term prevents the direct solution of equation (2.2) using single-electron wave functions and therefore it is necessary to introduce approximations to solve the equation. In the central field theory, it is assumed that the electrons move in a spherically-symmetric potential $U(r_i)$. Now the Hamiltonian is rewritten in the form

$$H = H_0 + H_1 \qquad (2.3)$$

where

$$H_0 = \sum_{i=1}^{N} \left\{ - \frac{\hbar^2}{2m} \nabla_i^2 + U(r_i) \right\} \qquad (2.4)$$

and

$$H_1 = \sum_{i>j} \frac{e^2}{4\pi\varepsilon_o r_{ij}} - \sum_{i=1}^{N} \left\{ \frac{Ze^2}{4\pi\varepsilon_o r_i} + U(r_i) \right\} \qquad (2.5)$$

It is assumed that $H_1$ which contains the effect of the non-central forces, is small compared to $H_0$ and hence $H_1$ is neglected in the zeroth approximation to solve the equation

$$H_0 \, \psi = \sum_{i=1}^{N} \left\{ - \frac{\hbar^2}{2m} \nabla_i^2 + U(r_i) \right\} \psi = E \, \psi \qquad (2.6)$$

By substituting a product of a single-electron eigen functions for $\psi$, the equation(2.6) is transformed into a separable set of Schrödinger equations for each electron:

$$\left\{ - \frac{\hbar^2}{2m} \nabla_i^2 + U(r_i) \right\} \psi_{nlm_l m_s}(i) = E_n(i) \, \psi_{nlm_l m_s}(i) \qquad (2.7)$$

The total energy is given by the sum of the single-electron energy eigen values,

$$E = \sum_{i=1}^{N} E_{nl}(i) \qquad (2.8)$$

The energy of a single electron in a central field depends only on n and l quantum numbers. Hence, the eigenfunction of the N-electron system is specified by a set of quantum numbers $\{n_1 l_1 \ldots n_N l_N\}$, defining the electron configuration. All the states $|n_1 l_1 m_{l_1} m_{s_1}, \ldots, n_N l_N m_{l_N} m_{s_N}\rangle$ belonging to the same configuration are degenerate with respect to the magnetic quantum numbers $m_{l_i}$ and $m_{s_i}$. This degeneracy is removed by the residual electrostatic interaction term $H_1$. In fact only the electrostatic repulsion term $\sum_{i>j} e^2/4\pi r_{ij}$ in $H_1$ acting on the valence electrons leads to the splitting of the degenerate states within a configuration. All the other terms in $H_1$ acting on the valence electrons or $H_1$ as a whole acting on the closed shells do not lift the degeneracy in a configuration but simply shift the total energy of the configuration. For a single configuration in

LS coupling approximation either $|LSM_LM_S>$ or $|LSJM_J>$ would be a suitable zeroth order representation for the perturbation $\sum_{i>j} e^2/r_{ij}$ and therefore the first-order shift in the energy is given by

$$\Delta E_1 = <\gamma LSM_LM_S \mid \sum_{i>j} \frac{e^2}{4\pi\varepsilon_o r_{ij}} \mid \gamma LSM_LM_S > \qquad (2.9)$$

$\Delta E$ is independent of the values of $M_L$ and $M_S$ and thus there is a $(2L+1)(2S+1)$-fold degeneracy with respect to $M_L$ and $M_S$. The set of $(2L+1)(2S+1)$ states labelled by L and S is called a term. These terms are further split into fine structure multiplets due to the spin-orbit interaction

$$H_2 = \sum_{i=1} \zeta(r_i) l_i \cdot s_i, \quad \zeta(r) = \frac{\hbar^2}{2m^2c^2} \cdot \frac{1}{r} \cdot \frac{dV}{dr} \qquad (2.10)$$

In LS coupling approximation, it is assumed that the splitting due to spin-orbit interaction is very much smaller than the separation between terms and hence $\sum_i \zeta(r_i) l_i \cdot s_i$ is treated as a perturbation within a single term. In degenerate perturbation theory, the zeroth-order wave functions demand a representation in which $H_2$ is diagonal. Even though, L and S and either $M_L, M_S$ or $J, M_J$ are good quantum numbers, representing constants of motion, $\gamma LSJM_J$ ($\gamma$ represents the configuration) forms a suitable representation in which $\sum \zeta(r_i) l_i \cdot s_i$ is diagonal. Then the first-order shift in energy is given by

$$\Delta E_2 = <\gamma LSJM_J \mid \sum_i \zeta(r_i) l_i \cdot s_i \mid \gamma LSJM_J> \qquad (2.11)$$

After a lengthy operator algebra, this expression can be transformed to

$$\Delta E_2 = \langle \gamma LSJM_J \mid \zeta(L,S) \ L.S \mid \gamma LSJM_J \rangle$$

$$= (1\backslash 2) \ \xi(L,S) \ \{ \ J(J+1)-L(L+1)-S(S+1) \ \} \qquad (2.12)$$

where $\xi(L,S)$ has the dimensions of energy and is constant within the levels of a given term. The effect of the spin-orbit interaction on a closed shell is easily shown to be zero. Each fine structure level of a term $(L,S)$ is often specified by a set of quantum numbers $(\gamma,L,S,J)$. Each energy level is still $(2J+1)$-fold degenerate with respect to the magnetic quantum number $M_J$. The energy difference between two adjacent levels in the same fine-structure multiplet is given by

$$\Delta E(J) - \Delta E(J-1) = \xi(L,S) \ J \qquad (2.13)$$

and is proportional to the value of J. This is known as the Lande interval rule and is useful for determining the J-values of the observed energy levels. The departure from this interval rule suggests the break down of the LS coupling approximation.

## II.3 HYPERFINE STRUCTURE INTERACTION

### II.3.1 General theory of hfs

The Coulomb and all the higher-order interactions between the electrons and the nucleus in an atom can be expressed in a compact form as a multipole expansion[10].

$$H = \sum_k T(e)^k . T(n)^k = T(e)^0 . T(n)^0 + H_{hfs} \qquad (2.14)$$

Where $T(e)^k$ and $T(n)^k$ are spherical tensor operators of rank k in the electronic and the nuclear space. By symmetry arguments of parity and time-reversal, the non-vanishing terms with even k-values represent electric and those with odd k-values magnetic

interactions. The monopole term (k=0) represents the coulomb interaction which specifies the interaction of the electrons with the spherical shape of the nuclear charge distribution. All the higher-order terms in the equation (2.14) contribute to the hyperfine structure(hfs). The major contributions to the hfs are from the nuclear magnetic dipole moment interacting with the magnetic field (k=1 term) and the nuclear quadrupole moment interacting with the electric field gradients (k=2 term). All the higher-order terms ($k{\geq}3$) are usually negligibly small. For example, the magnetic octupole (k=3) and electric hexadecapole (k=4) interactions are about $10^8$ times smaller than their corresponding lower order magnetic dipole(k=1) and electric quadrupole(k=2) interactions.

The general theory of hyperfine interaction is briefly described here using non-relativistic perturbation methods. The hyperfine coupling constants are derived in terms of the electromagnetic fields and nuclear moments.

## II.3.2 Magnetic Dipole Interaction

The first major contribution comes from the coupling of the magnetic dipole moment $\vec{\mu}_I$ of the nucleus having a non-zero nuclear spin I with the magnetic field $\vec{H}_J(0)$ produced by the electrons at the vicinity of nucleus. The interaction Hamiltonian is written as a scalar product of nuclear and electronic tensors, each of rank one

$$H_M = - \vec{\mu}_I \cdot \vec{H}_J(0) \tag{2.15}$$

The magnetic field at the nucleus is produced by both the orbital

motion and the spin dipole moment of the electrons. From symmetry arguments, this field is linearly related to the total angular momentum of the electrons $\vec{J}$ which is specified as $\vec{J}=\vec{L}+\vec{S}$. The nuclear magnetic moment can be written as

$$\vec{\mu}_I = \mu_N g_I \vec{I} = \frac{\mu_I}{I} \vec{I} \qquad (2.16)$$

where $\mu_N$ is the nuclear magneton, $g_I$ the nuclear g-factor and $\mu_I$ the nuclear moment. In IJ approximation, I and J are good quantum numbers and hence the interaction Hamiltonian may be written in the form

$$H_M = hA \; \vec{I}.\vec{J} \qquad (2.17)$$

where A is the magnetic dipole coupling constant which is equal to $-\frac{\mu_I H_J(0)}{hIJ}$.

An additional term called the Fermi-contact term arises for an s-electron($l=0$) which has a non-zero probability density at the origin $|\psi(0)|^2$. The unpaired s-electron in penetrating orbit interacts with the nuclear magnetic moment $\mu_I$. Therefore the magnetic interaction

$$H_M = a_s \; \vec{I}.\vec{S} = a_s \; \vec{I}.\vec{j} \qquad (2.18)$$

where

$$a_s = \left( 2\mu_B \frac{\mu_I}{I} \right)\left( \frac{8\pi}{3} \right) \; |\psi(0)|^2, \quad l=0 \qquad (2.19)$$

For an isolated J level ( fine structure level), $H_M$ is treated as a perturbation which is diagonal in the $|IJFM_F\rangle$ representation, where $\vec{F}=\vec{I}+\vec{J}$. The quantum number F describes the total angular momentum of the atom which is a constant of motion. Hence, the

first-order energy shift of a level J is written as

$$\Delta E_M = < \gamma IJFM_F \mid hA \: I.J \mid \gamma IJFM_J >$$

$$= \frac{hA}{2} \: K, \quad ( \: I \geq 1/2, \: J \geq 1/2 \: ) \qquad (2.20)$$

where $K=F(F+1)-I(I+1)-J(J+1)$. The splitting into hyperfine structure levels are specified by F which are (2F+1) fold degenerate. The quantum number F has 2I+1 values for I≤J or 2J+1 values for J≤I. The coefficient A which is a measure of the splitting, obeys the interval rule

$$\Delta E \: (F) \: - \: \Delta E \: (F-1) \: = \: hAF \qquad (2.21)$$

and will be the largest for unpaired s-electrons which penetrate the nucleus.

## II.3.3  Electric Quadrupole Interaction

The quadrupole interaction arises due to the coupling between the nuclear quadrupole moment $\vec{Q}_I$ and the electric field gradient $\vec{q}_J(0)$ at the nuclear site. According to equation (2.14), the interaction Hamiltonian is written as

$$H_E = \vec{Q}_I \: . \: \vec{q}_J(0) \qquad (2.22)$$

$\vec{Q}_I$ and $\vec{q}_J$ are tensor operator of rank two. In IJ coupling approximation, it is assumed that the directions of $\vec{I}$ and $\vec{J}$ establish the axes of cylindrical symmetry for the quadrupole moment and the electric field gradient tensors respectively. In this approximation where the matrix elements are diagonal with respect to I and J equation(2.22) reduces to

$$H_E = hB \frac{\left[ 3(\vec{I}.\vec{J})^2 + (3/2)\vec{I}.\vec{J} - I(I+1) J(J+1) \right]}{2I(I-1) J(2J-1)} \tag{2.23}$$

where $B = e^2 Q_I q_J(0)$ is the electric quadrupole coupling constant. In $|IJFM_F\rangle$ representation, the first-order energy shift of a fine structure level J is

$$\Delta E_E = \langle IJFM_F | H_E | IJFM \rangle$$

$$= \frac{hB}{4} \frac{3/2 \ K(K+1) - 2I(I+1)J(J+1)}{I(2I-1)J(2J-1)}, \quad (I \geq 1, J \geq 1) \tag{2.24}$$

This interaction vanishes for S terms, because $q_J(0)$ vanishes when the electron charge distribution is spherically symmetric. The interaction also vanishes for I=0 or 1/2 because the nulear charge ditribution is spherically symmetric and therefore the quadrupole moment $Q_I$ is identically zero. Though the contribution from this interaction to the hyperfine structure is usually small it is a significant factor in the case of highly deformed nuclei.

The total hfs-energy of a free atom is the sum of the energies (2.20) and (2.24)

$$E_F = \frac{hA}{2} K + \frac{hB}{4} \frac{(3/2) \ K(K+1) - 2I(I+1) \ J(J+1)}{I(2I-1) \ J(2J-1)} \tag{2.25}$$

which is the well-known Casimir formula. It is evident from eqn.(2.25) that the contribution from quadrupole interaction leads to the departure from the interval-rule because the contribution depends on F in a nonlinear fashion. From the Casimir formula one can infer that the centre of gravity of a level J does not shift due to the hyperfine splittings since

$$\sum_F (2F+1) E_F = 0 \tag{2.26}$$

The selection rules for the dipole transitions between two hfs-multiplets follows

$$\Delta I = 0, \quad \Delta J = 0, \pm 1, \quad \Delta F = 0, \pm 1 \quad (\text{ but not } 0 \leftrightarrow 0 ) \qquad (2.27)$$

The relative intensities among the hyperfine components of a transition are commonly derived from the sum rule. This rule states that the sum of the intensities of all the components from an initial level or to a final level of a multiplet is proportional to the statistical weight (2F+1), of that level; the constant of proportionality is common to all the levels of a given multiplet. Using the degeneracies of both initial and final levels, a set of simultaneous equations can be formed and solutions of these equations give the relative intensities. These intensities are tabulated in many books[11,4] for transitions between different electronic total angular momenta and for different nuclear spins.

## II.3.4 Effective Operator Formalism

The hyperfine interaction depends significantly on the electron wavefunctions in the neighbourhood of the nucleus. Since the velocities of the electrons in this region is comparable to the velocity of light, the electrons should be described by relativistic Dirac wave functions. The relativistic effects are therefore predominent in the heavier atoms. Unfortunately, the relativistic calculations are generally much more difficult to carry out than non-relativistic calculations. In 1965 Harvey[15] has introduced a novel technique for the analysis of hfs spectra in terms of an "effective Hamiltonian". It was found that three

operators are necessary to use in the hyperfine Hamiltonian. With such a Hamiltonian it is possible to include all types of configuration-interaction effects (polarization and correlation) that can be described by a one-body effective operator. Later Sandars and Beck [16] have introduced an effective-operator formalism for the relativistic hyperfine interaction according to which the matrix elements of the true Hamiltonian H between LS-coupled relativistic eigen functions are equal to the matrix elements of an effective Hamiltonian $H_{hfs}^{eff}$ between non-relativistic LS-coupled states within a given configuration. This effective Hamiltonian is of the same form as (2.14) for $H_{hfs}$ and is written as

$$H_{hfs}^{eff} = \sum_{k=1}^{\infty} T_{eff}^{k}(e) \cdot T^{k}(n) \tag{2.28}$$

In $|IJFM_F\rangle$ representation, the hfs energy of an atomic state is given as the first order expectation value of $H_{hfs}$

$$E_F = \langle IJFM \mid H_{hfs} \mid IJFM \rangle$$

$$= \sum_{k=1}^{2} (-1)^{J+I+F} \begin{Bmatrix} I & J & F \\ J & I & K \end{Bmatrix} \langle J||T(e)^k||J\rangle \langle I||T(n)^k||I\rangle \tag{2.29}$$

The reduced matrix elements are independent of the magnetic quantum number M. The degeneracy in F is removed by the hyperfine interaction and the F dependence is entirely contained in the 6-J symbol and a phase factor. The 3-J and 6-J symbols are tabulated by Cowan [17].

When fine structure levels of different J are very widely seperated, both I and J are considered as good quantum numbers. Equation (2.29) is also expressed in the form [10]

$$E_F = \sum_{k=1}^{2} A_k \, M(IJ;F;k), \quad [M(IJ;I+J;k)] = 1 \qquad (2.30)$$

where $A_k$ are given by

$$A_k = \langle JJ|T^k(e)|JJ\rangle \, \langle II|T^k(n)|II\rangle \qquad (2.31)$$

By the application af Wigner-Eckart theorem the parameters $A_k$ are related to the matrix elements of equation (2.29) as

$$A_k = \begin{pmatrix} J & k & J \\ -J & 0 & J \end{pmatrix} \langle J\|T(e)^k\|J\rangle \begin{pmatrix} I & k & I \\ -I & 0 & I \end{pmatrix} \langle I\|T(n)^k\|I\rangle \qquad (2.32)$$

The expressions in the parentheses is a 3-j symbols whereas $\langle II|T(n)^1|II\rangle = \mu_I$ and $\langle JJ|T(e)^2|JJ\rangle = q_J$. Combining equations (2.29), (2.31) and (2.32) and using the explicit formulae for 6-j and 3-j symbols, one gets the popular Casimir formula (2.25) when $A_1 = AIJ$ and $A_2 = B/4$ are substituted.

The hyperfine constants A and B are then related to the effective tensor operators $T(e)^1$ and $T(e)^2$ through the reduced matrix elements

$$A = \frac{\mu_I}{I} \left[ J(J+1)(2J+1) \right]^{-1/2} \langle J\|T(e)^1\|J\rangle \qquad (2.33a)$$

and

$$B = 2eQ_I \left[ \frac{2J(2J-1)}{(2J+3)(2J+3)} \right]^{1/2} \langle J\|T(e)^2\|J\rangle \qquad (2.33b)$$

The expressions for the electric effective tensor operators can be explicitly written as [12,13]

$$T(e)^1 = 2\mu_0 \sum_{i=1}^{N} \left[ \vec{l}_i \langle r_i^{-3}\rangle_{01} - \sqrt{10} \, (\vec{s}_i * \vec{c}_i^2)^1 \langle r_i^{-3}\rangle_{12} + \right.$$

$$\left. \vec{s}_i \langle r_i^{-3}\rangle_{10} \right] \qquad (2.34a)$$

$$T(e)^2 = e\sum_{i=1}^{N} \left[ -\vec{c}_i^{\,2} \langle r_i^{-3} \rangle_{02} + \left\{ \vec{s}_i * (\vec{c}_i^{\,4} * \vec{1}_i)^3 \right\}^2 \langle r_i^{-3} \rangle_{13} + \right.$$

$$\left. (\vec{s}_i * \vec{1}_i)^2 \langle r_i^{-3} \rangle_{11} \right] \qquad (2.34b)$$

The summation extends over all electrons in open shells. In these expressions $\vec{1}$ and $\vec{s}$ are the orbital and spin moments and $\vec{C}^2$ and $\vec{C}^4$ are tensor operators closely related to spherical harmonics. Radial integrals $\langle r_i^{-3} \rangle$ are similar to $\int R(r)(1/r_i^3)R(r)r^2 dr$, where $R(r)$ is the radial part of the electronic wave function. The radial integrals $\langle r_i^{-3} \rangle_{01}$, $\langle r_i^{-3} \rangle_{12}$, $\langle r_i^{-3} \rangle_{10}$ and $\langle r_i^{-3} \rangle_{02}$ represent orbital, spin-dipole, Fermi-contact and quadrupole interaction terms respectively. In the non-relativistic limit $\langle r_i^{-3} \rangle_{01} = \langle r_i^{-3} \rangle_{12} = \langle r_i^{-3} \rangle_{02} = \langle r_i^{-3} \rangle_{nl}$ (l>0) for non-s electrns and $\langle r^{-3} \rangle_{10} = 4\pi\delta(r) \neq 0$ only for s-electrons. The radial integrals $\langle r_i^{-3} \rangle_{13}$ and $\langle r_i^{-3} \rangle_{11}$ are purely relativistic and vanish in the non-relativistic case. Therefore the quadrupole interaction is entirely orbital in nature.

It is not straightforward but rather difficult to calculate the radial integrals appearing in equation (2.33) and therefore they are often interpreted as three radial hyperfine parameters

$$a_{10}(i) = -\frac{4}{3} \frac{\mu_0}{4\pi} \mu_B \frac{\mu_I}{I} \langle r_i^{-3} \rangle_{10} \qquad (2.35a)$$

$$a_{kl}(i) = 2 \frac{\mu_0}{4\pi} \mu_B \frac{\mu_I}{I} \langle r_i^{-3} \rangle_{kl} \qquad (2.35b)$$

$$b_{kl}(i) = \frac{e^2}{4\pi\varepsilon_0} Q_I \langle r_i^{-3} \rangle_{kl} \qquad (2.35c)$$

These parameters are generally determined from a least-squares fit to the experimental hfs constants, treating the hyperfine parameters as adjustable parameters. For the analysis of this kind, the hfs constants for atleast three states in the same LS term or configuration must be known. If the magnetic dipole moment is also known it is possible to evaluate the hyperfine radial integrals. These experimentally determined integrals can be compared with the theoretically evaluated hyperfine radial integrals to test the hyperfine theory. The electric quadrupole moment can be calculated from the experimental $b_{kl}$ parameters using theoretical hyperfine radial integrals. The evaluation of matrix elements in equation(2.33) for obtaining the parametrized hfs constants is quite tedious. Often one uses big computer programs with accurately calculated wave functions as inputs for evaluating these matrix elements.

## REFERENCES

1.  A.Michelson, Phil.Mag.31, 338(1891).

2.  C.Fabry and A.Perot, Ann.Chim. Phys.12, 459(1897).

3.  O.Lummer and Gehrcke, Ann.Phys.10, 457(1903).

4.  E.U.Condon and G.H.Shortly, The Theory of Atomic Spectra(Cambridge University Press, 1964).

5.  W.Pauli, Naturwissenschaften 12, 74(1924).

6.  H.Schüler and T.Schmidt, Z.Physik 94, 457(1935).

7.  H.B.G. Casimir, on the Interaction between Atomic Nuclei and Electrons(Teyler's Tweede Genootschap, Harlem, 1936).

8.  V.Jaccarino, J.G.King, R.A.Satten and H.H.Stroke, Phys.Rev. 94, 1798(1954).

9.  H.Figger, G.Wolber and S.Penselin, Phys.Lett.34A, 21(1971).

10. C.Schwartz, Phys.Rev. 97, 380(1955).

11. H.Kopfermann, Nuclear Moments(Academic Press, New York, 1958).

12. L.Armstrong Jr., Theory of the Hyperfine Structure of Free Atoms(Wiley-Interscience, New York, 1971).

13. I.Lindgren and A.Rosen, Case Stud. At. Phys.4, 93(1974).

14. G.K.Woodgate, Elementary Atomic Structure(Clarendon Press, Oxford, 1980).

15. J.S.M.Harvey, Proc. Roy. Soc. (London) A285, 581(1965).

16. P.G.H.Sandars and J.Beck, Proc.Roy.Soc.(London)A289, 97(1966)

17. R.D.Cowan, The Theory of Atomic Structure and Spectra(University of California Press, 1981).

CHAPTER III

OPTOGALVANIC SPECTROSCOPY-EXPERIMENTAL DETAILS

### III.1 INTRODUCTION

The introduction of laser as a spectroscopic tool has dramatically altered the field of optical spectroscopy. It has not only renewed the conventional optical spectroscopic techniques but has led to the development of many powerful new spectroscopic techniques. There are several interesting properties of lasers that have made them valuable for the spectroscopic investigation. The intensity, monochromaticity, coherence, polarization and tunability of lasers make it possible to investigate the atomic spectroscopy with many orders of magnitude more sensitivity and selectivity than was possible previously. The high spectral densities and purities of lasers have made possible the development of important spectroscopic techniques like saturation spectroscopy and multiphoton spectroscopy. The advent of tunable dye-lasers has given new impetus to atomic fluorescence spectroscopy and optogalvanic spectroscopy, especially with regard to detection limits.

### III.2 OPTOGALVANIC SPECTROSCOPY

### III.2.1 Introduction

Optogalvanic spectroscopy (OGS) is based on the "Optogalvanic effect" which is the change in the impedance of a gaseous discharge due to the resonant light absorption. It is a simple and

convenient detection technique to study the spectroscopy of atoms, ions, molecules and radicals in electrical, high-frequency discharge plasmas and flame plasmas [1-4]. OGS is a very sensitive detection technique and makes it possible to detect transitions which are not detectable in absorption or fluoresence spectroscopy. Unlike emission or absorption spectroscopy which require the use of optical detectors, OGS does not require an additional detector, instead the discharge plasma itself acts as a sensitive non-optical detector of the optical phenomena. No background filtering is needed in the OGS and the signal-to-noise ratio is generally of the order of $10^3$.

Optogalvanic effect is known for more than five decades. Early work on the effect was performed by many authors, Foote and Mohler in 1925[5], Penning in 1928[6], Joshi in 1944[7], Kenty in 1950[8], and Meissner and Miller in 1953[9] all using incoherent light sources. The development of tunable dye lasers opened many new possibilities and the optogalvanic effect became widely popular as a detection method in laser spectroscopy.

III.2.2  A simple theory of optogalvanic effect

A qualitative explanation of the optogalvanic effect is fairly straightforward. There are two significantly different mechanisms for the origin of the optogalvanic effect in hollow cathode discharges[10]. In the first mechanism, the absorption of laser radiation in the discharge results in a change in the steady state population of bound atomic or molecular levels. Different levels will generally have different ionization rates or

ionization probabilities. Hence there is a net change in the ionization balance of the discharge. A perturbation to the ionization balance leads to a change in the current through the discharge or, equivalently, a change in the impedance of the discharge. In the second mechanism, the excitation of atoms by the laser to higher electronic states perturbs the equilibrium established between the electronic temperature and the atomic excitation temperature. But the superelastic collisions between the electrons and the laser-excited atoms in the discharge tend to restore the equilibrium. In this process an excess amount of energy is released which often end up in an increased electron temperature of the discharge. Therefore the laser excitation of atoms leads to the increase in the conductivity or decrease in the impedance of the discharge. In fact, both the mechanisms are expected to be present simultaneously in the OGS. The relative importance of these two mechanisms depends on different discharge and excitation conditions. Although a qualitative explanation is straight forward, a detailed quantitative description of the optogalvanic effect is much more difficult. Quantitative treatments generally involve applying perturbation theory to a model of the unperturbed discharge. There are many such attempts made by several authors[11-14] recently. However, full agreement between the theory and the experimental results is not achieved.

A phenomenological simplified theory for optogalvanic effect was presented by Eraz et.al[15] in 1979. Using this theory, the relative magnitudes, signs, and time evolution of the optogalvanic signals can be explained qualitatively in cases of chopped cw

laser and pulsed laser excitation.

In the phenomenological theory a dc discharge tube in series with a ballast resistor is considered. The buffer gas pressure and the discharge current are maintained such that it forms a positive internal tube resistance. A multiplication factor $\alpha$ is defined as the number of electrons generated at the cathode by the avalanche caused by a single electron emitted from the cathode. If $\alpha > 1$, the discharge current increases and the voltage drop across the ballast resistor increases. This causes the voltage across the tube decrease and hence a decrease in $\alpha$ (self-regulation). In an optogalvanic experiment, the laser beam illuminates certain discharge region through which the electrons pass. In the small-signal domain, the quasi-stationary conditions demand $\alpha \equiv 1$ Therefore

$$d\alpha = \left( \frac{\delta\alpha}{\delta V} \right)_{n_i} \Delta V + \Sigma \left( \frac{\delta\alpha}{\delta n} \right)_{V, n_j}{}_{j=i} \Delta n_i = 0 \qquad (3.1)$$

where $V$ is the voltage across the tube, $\Delta V$ is the deviation in the voltage from the steady state (optogalvanic signal), $n_i$ are the various atomic and ionic populations and $\Delta n_i$ are the deviations in the populations from steady state. From equation (3.1)

$$\Delta V = -\beta \Sigma a_i \Delta n_i \qquad (3.2)$$

where $\beta = \left( \frac{\delta\alpha}{\delta V} \right)_{n_i}^{-1}$ and $a = n\left( \frac{\delta\alpha}{\delta n} \right)_{V, n_j}$. Qualitatively it can be shown that $\beta$ is always positive since an increase in the voltage increases the ionization probability. Generally $a_i$ increases for higher energy states and $a_i > 0$ for all i. The rate equations can be written as

$$\frac{d(\Delta n_1)}{dt} = - \frac{\Delta n_1}{T_1} - (n_1 - n_2) \, \sigma_{12} \, I_{12} \tag{3.3a}$$

$$\frac{d(\Delta n_2)}{dt} = - \frac{\Delta n_2}{T_1} - (n_2 - n_1) \, \sigma_{12} \, I_{12} \tag{3.3b}$$

These equations can be used to deduce the behaviour of the optogalvanic signal for both cw and pulsed modes of laser illumination. For cw laser excitation $\frac{d(\Delta n)}{dt} = 0$ and the equation (3.3) becomes

$$\Delta n_1 = -(n_1 - n_2) \, \sigma_{12} \, I_{12} \, T_1 \tag{3.4a}$$

$$\Delta n_2 = (n_1 - n_2) \, \sigma_{12} \, I_{12} \, T_2 \tag{3.4b}$$

combining equation (3.2) and (3.4) one obtains

$$\Delta V = -\beta \, \sigma_{12} \, I_{12} \left\{ a_2 T_2 - a_1 T_1 \right\} (n_1 - n_2) \tag{3.5}$$

Assuming $E_1 < E_2$, $n_1 > n_2$ and $a_2 > a_1$ one can make the following deductions.

(1) The optogalvanic signal $\Delta V$ is always negative unless $a_1 T_1 > a_2 T_2$. The absorption of radiation in the discharge produces a transition to a higher state, from which collisional ionization proceeds more easily and hence the discharge impedance and voltage across the discharge tube decrease. This represents a negative optogalvanic signal. Conversely excitation from metastable states produces the positive optogalvanic signals. Depletion of long-lived states, from which the atoms can be ionized more easily by collisions leads to an increase in the discharge impedance and voltage across the discharge tube. The relaxation times are very sensitive to the plasma conditions. Increasing current or pressure can change the sign of a signal from positive to negative due to a

decrease in $T_1$ caused by enhanced electron collisions.

(2) The time profile of $\Delta V$ will be the same as that of $\sigma_{12}$.

(3) In the small signal limit, the magnitude of the optogalvanic signal $\Delta V$ is proportional to $(n_1 - n_2)$ and $\sigma_{12} I_{12}$.

### III.2.3 OGS of sputtered atoms

The optogalvanic detection technique is well suited to spectroscopic studies with sputtered atoms for several reasons. The atomic spectroscopy of refractory and non-volatile elements can be carried out with ease with this method. High resolution spectroscopy of sputtered atoms is often preferred since the Doppler widths of the spectral lines for sputtered atoms are usually narrow [16].

The hollow cathode discharge serves as a rich reservoir of sputtered atoms. Under the right conditions of gas pressure and bore diameter of the cathode, the negative glows from opposite walls of the inner surface of the hollow cathode coalesce to produce neutral and excited atoms and ions in high densities at the centre of the hollow cathode. The hollow cathode discharge is highly self-sustaining as it sustains large currents at cathode-fall potential of only a small voltage.

Applying a potential difference of a few hundred volts between the two electrodes leads to breakdown of the rare gas at low pressure and creation of a number of electron-ion pairs. The ions are accelerated in the high field of the cathode dark space and bombard the cathode material together with fast neutral atoms produced by resonant charge exchange. The high energetic ions and

fast neutral atoms impart sufficient energy to the crystal lattice of the cathode material to dislodge and eject the atoms from the lattice sites. The sputtered species, predominantly single, ground state neutral atoms, which initially posess high kinetic energies, rapidly lose their kinetic energy by elastic collisions with rare gas atoms and come into thermal equilibrium[17]. As the sputtered atoms diffuse from the cathode surface into the negative glow, some of them are excited or ionized by electron impact or by collisions with metastable atoms or ions present in the discharge. In this way, reasonably high steady-state densities of ground-state atoms, metastable atoms and singly-ionized ions can be accumulated in the nagative-glow region of the discharge suitable for carrying out optogalvanic spectroscopy.

### III.3  EXPERIMENTAL DETAILS

### III.3.1  CW optogalvanic spectroscopy

The experimental arrangement used for all the fine structure investigations carried out in this thesis is shown in Fig. III.1. A standing wave cavity dye laser (Spectra Physics 375A) with Rhodamine 6G dye solution was pumped by a 5Watt argon ion laser (Spectra Physics 2020 ). At 4Watt of all lines pump power, a typical dye output power of 600mW was obtained in the wavelength range 570-640nm. Smooth scanning of the wavelength was accomplished by rotating the micrometer of the birefringent filter in the dye laser by an 1/2 rpm synchronous motor.

The output of the dye laser is focussed into the hollow cathode of a discharge lamp by a condensing lens (f=10cm). The dye
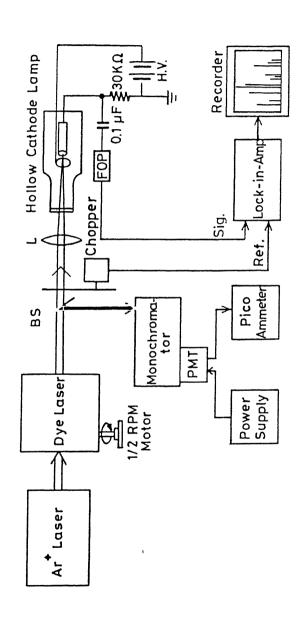
**Fig. III.1 EXPERIMENTAL ARRANGEMENT FOR OPTOGALVANIC SPECTROSCOPY**
FOP-fast over voltage protection; PMT-photomultiplier tube

laser beam is chopped by a mechanical chopper(Ithaco 220A) to facilitate phase sensitive detection through a lock-in amplifier. The chopping frequency is chosen such that the noise is minimum. The discharge in the hollow cathode lamp is struck and maintained with the help of a well regulated high voltage power supply (Aplab 7323). Most often it was found possible to obtain a stable discharge (with constant current) in a hollow cathode lamp with a ballast resistor of $30k\Omega$ or higher connected in series with the hollow cathode. The optogalvanic signals were picked up through a dc-blocking capacitor of $0.1\mu F$ and a fast over voltage protection circuit and were fed to the voltage input terminal of a lock-in amplifier (SR 510). The reference signal (4volt peak-to-peak square wave)for the lock-in amplifier was also obtained from the chopper. The lock-in amplifier amplifies the signals which appear at reference frequency and are in phase with reference signals and averages all the asynchronous signals which are mostly noise. In this way a significant increase in signal-to-noise ratio is obtained. The output of the lock-in amplifier is fed to a strip chart recorder

The wavelength of the dye laser is generally monitored by a double monochromator (Spex 1402). The resolution of the monochromator is about $0.1\overset{\circ}{A}$ at slit widths of about $20\mu m$. A photomultiplier tube (FW 130) was fixed to the exit slit of the monochromator to detect the diffracted light. A picoammeter (Keithley 417) was employed to measure the output current of the photomultiplier tube.

## III.3.2  Doppler-limited high resolution OGS

A schematic of the experimental set-up is shown in Fig.III.2. The set-up is similar to the one given in Fig.III.1 except for the 18Watt Argon ion laser(Spectra Physics 171) and single frequency ring dye laser(Spectra Physics 380D). The pump laser was operated at 514.5nm using a prism assembly. The green output with $TEM_{00}$ mode was used to pump the ring dye laser with Rhodamine 6G dye. With 4Watt of 514.5nm pump, about 400mW single-frequency dye output was obtained routinely. The frequency of the ring dye output is actively stabilized by an external reference station and it can be scanned over 30GHz with the help of stabilock electronics. The linewidth of the laser is often less than 3MHz. The frequency of the laser is monitored during scans by a Fabry-Perot interferometer(Coherent 216) with 300MHz FSR. The frequency markers were also recorded simultaneously with the signals.
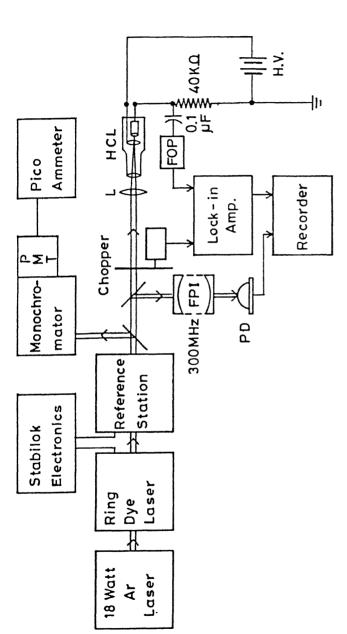
## III.4  THE DYE LASER

### III.4.1  Introduction

Dye lasers are tunable light sources used extensively in the atomic spectroscopy experiments. A brief description of the principles of the dye laser operation, and frequency stabilization and scanning is given here with special reference to the dye lasers used in the present experiments.

### III.4.2  Operation
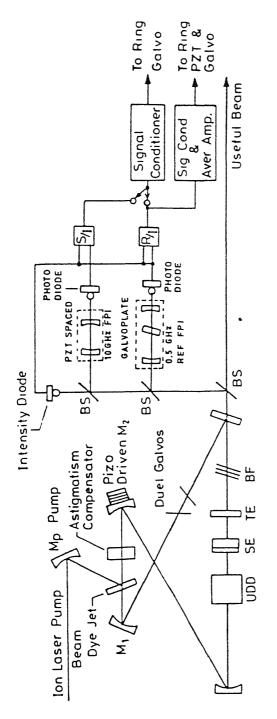
In cw dye lasers a continuous flowing jet of dye solution is used as a gain medium. In the experiments conducted here Rhodamine

FIG.III.2 EXPERIMENTAL SET-UP FOR DOPPLER-LIMITED HIGH RESOLUTION OPTOGALVANIC SPECTROSCOPY

BS-beam splitter; HCL-hollow cathode lamp; FOP-fast over voltage protection; HV-high voltage power supply; PMT-photomultiplier tube; FPI-Fabry-Perot interferometer; PD-photodiode

6G dye in ethylene glycol and methanol solutions was used. The dye (Rhodamine 6G) molecules are excited from the electronic ground state to the first excited electronic singlet state by the absorption of pump-laser. The electronic energy levels of the dye are considerably broadened because of the large number of vibrational-rotational levels associated with them. After the fast nonradiative relaxation down to the lowest vibrational level of the singlet state, the dye molecules decay to different rotational-vibrational levels of electronic ground state. Since the rotational-vibrational lines which are closely spaced are collision broadened due to the strong interaction of the dye molecules with the solvent, the emitted fluorescence spectra completely overlap and produce a broad continuum. This emitted light passes through the dye stream many times as it is reflected back and forth by the mirrors of the optical cavity of the dye laser. In this process the fluorescence stimulates the dye molecules already excited by the pump laser to emit light at the fluorescence wavelengths, providing the lasing action. The accumulation of dye molecules in the metastable triplet state through singlet-to-triplet intersystem crossings often hampers the lasing action. This can be avoided by pumping the dye solution at high speed through the lasing region. For Argon ion laser pumping, Rhodamine 6G dye generally provides laser gain from 560 to 640 nm. The schematic of the ring dye laser (SP 380D) is shown in Fig.III.3. Unlike the traditional standing wave cavity dye lasers the ring dye laser is a travelling-wave ring-resonator cw dye laser. Since the light waves propagate around cavity continuously,

FIG.III.3   SCHEMATIC OF THE RING DYE LASER(SP 380D)

UDD. Uni Directional Device
SE: Scanning Etalon
TE: Thin Etalon
BF. Birefringent Filter
BS: Beam Splitter

all the dye molecules receive feedback radiation and thus the spacial hole-burning is avoided. Extraction of the entire dye volume by the travelling waves enable a single cavity mode to compete for excited state molecules in entire dye jet regions. The unidirectional device in the cavity allows the travelling waves to propagate in only one direction. The result is that the output power is quite high and is concentrated in a single beam with a narrow line width.

### III.4.3  Single frequency selection

The selection of single frequency in the ring dye laser is easy because of the high single frequency conversion efficiency. The longitudinal mode spacing of the ring cavity is about 200 MHz. Since the emission gain curve of the dye laser extends over several hundreds of angstroms, simultaneous lasing can occur at a large number of cavity modes. Single frequency operation is obtained by insertion of many frequency selective elements inside the ring cavity: a birefringent filter, a thick etalon and a fine etalon. The relative band-pass of the various tuning elements are shown in Fig.III.4. The spectral ranges of the tuning elements are chosen such that loss is introduced beyond the threshold for all the cavity modes except the particular one where the lasing is desired.

### III.4.4  Frequency stability and scanning

Due to ambient pressure variations, acoustic and mechanical disturbances and variations of the dye jet thickness, optical path length of the cavity changes forcing the free running laser to

have an effective linewidth of 20MHz. Mode-hops can also be caused by extensive vibrations, microphonics in the cavity and bubbles passing through the dye jet. These drawbacks would limit the usefulness of the laser for high resolution spectroscopy. To reduce the linewidth as well as to prevent the mode-hops the frequency of the ring dye laser is stabilized by locking it to a fringe of an interferometer(FSR=0.5MHz). Reference interferometer operates over the entire visible and near-IR spectral regions, and provides the highest possible rate of change of transmission as a function of frequency. Thus any variation in the frequency of the laser varies the intensity of light transmitted through the reference interferometer. This variation is detected by the reference photodiode. The signal from this diode is normalized to the signal of the intensity diode which monitors the laser output power and is used to generate the error signal. The error signal is immediately fed back to PZT-mounted mirror($M_2$) and the double galvoplates in the ring cavity to correct the variation in the frequency. Since the cavity spacing in the ring dye laser is 200MHz, a mode-hop of only two cavity modes tends the laser frequency to lock to another fringe of the reference interferometer. This is overcome by monitoring the laser frequency with a second interferometer(slave) with an FSR of 10GHz. When the laser tries to mode-hop, the slave interferometer circuitry takes control and returns the laser frequency to the original fringe of the reference interferometer. Under the normal circumstances the slave interferometer is passive. With the help of stabilock electronics the locking point is chosen as shown in Fig. III.5.
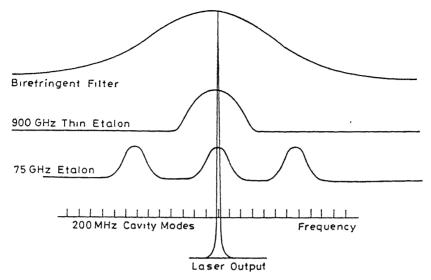
Fig.III.4 Single frequency selection in ring dye laser.
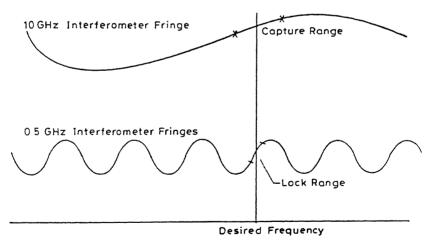


Fig. III.5 Frequency locking of laser to external etalons.

With this double interferometer stabilization system the laser linewidth is reduced to less than 1MHz.

The birefringent filter is used for coarse wavelength tuning and selects a frequency band of operation. The thick etalon (FSR=75GHz) selects a single cavity mode within this frequency band. With all the tuning elements inside the cavity,the single frequency output of the ring dye laser can be scanned over a range of 30GHz with the help of double galvoplates and scanning thick etalon. Since the frequency of the stabilized laser is controlled by the external interferometers, these interferometers must be scanned to change the laser frequency. The 0.5GHz interferometer is scanned by rotating a galvo-mounted quartz plate inside the interferometer cavity, whereas the 10GHz interferometer is scanned by moving one of its mirrors mounted on a PZT. In this way a mode-hop-free scanning of over 30GHz is possible. If a mode hop occurs during the scan, both the 0.5GHz and 10GHz interferometers momentarily stop scanning and continue soon after the frequency is brought back to the correct fringe of the 0.5 GHz interferometer by the double galvoplates.

## III.5 TEST STUDIES

### III.5.1 OGS of Neon and Uranium

The optogalvanic spectra of neon and uranium were obtained for calibration and optimization purposes. Since these two elements have a number of strong well studied lines[18,19] in the spectral region (R6G dye range) of interest, their spectra were used for calibration purposes. Incidentally neon is the buffer gas

common in all the hollow cathode lamps studied, and hence the neon lines recorded simultaneously in the experiments provided convenient calibration lines. The characteristics of optogalvanic signals are verified by these studies.

Typical optogalvanic spectra of (Na/Ne) and (U/Ne) are given in Fig.III.6 and Fig.III.7 respectively. The experimental set-up used for recording these spectra is same as the one described in Fig.III.1. Two commercial hollow cathode lamps, Na/Ne (Hamamatsu) and U/Ne (Instrumentations Laboratories Inc) were used in these studies. They were operated at the discharge currents of 6mA and 15mA respectively. In the case of Na/Ne, the chopping frequency was held fixed at 440Hz and the dye laser peak power was kept constant at 160mW. In the case of U/Ne, the laser beam was chopped at 230Hz and the laser peak power was fixed at 190mW while the laser was scanned in the range of 5680-6340 Å.

As seen from the observed spectra, many of the optogalvanic signals are positive because the corresponding transitions originate from metastable states. The behaviour of the optogalvanic signals of some transitions with discharge current and laser power are shown in Fig.III.8, Fig.III.9 and Fig.III.10. These data were used to decide the optimal operating conditions with minimum signal distortion.

### III.5.2  OGS of Rubidium in dc discharge

Optogalvanic effect in the positive column of a dc glow discharge was studied in the OGS of rubidium in a dc discharge. A discharge tube with 4mm internal diameter and a 10cm active length

OG Signal Intensity (arb. units)

5801.752 (K) 5804.449
5811.406
5816.645
5820 155
5828.910
5831.887 (K)
5852.487
5868.418 5872 149
5872 827
5881.895
* 5895 923 (Na)
* 5889.590 (Na)
5898.406
5902.462
5906 429
5913 270
5918.906
5932.401
5934 458
5939.319
5944.834
5961.622
5965.471
5966.171
5974.627
5975.534
5987 907
5991.653
6000.927
6029 997
6042.013
6046.134

Wavelength (Å)
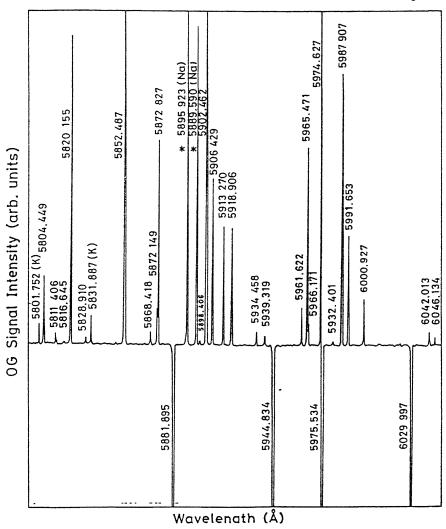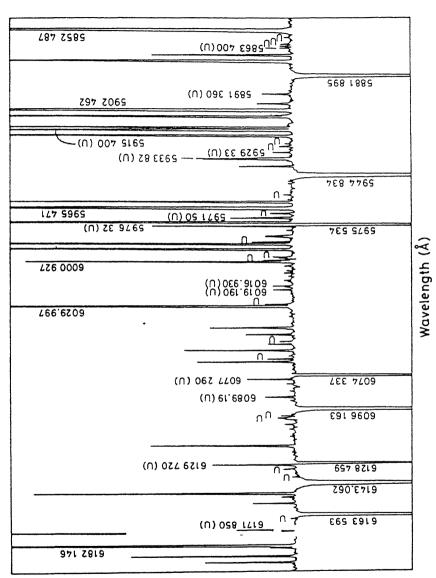
FIG.III.6  A TYPICAL OPTOGALVANIC SPECTRUM OF NEON

Spectral lines other than neon are indicated. The graph is linear to the first order.

FIG. III.7  A TYPICAL OPTOGALVANIC SPECTRUM OF URANIUM AND NEON

Some of the strong uranium lines as well as neon lines used for calibration are marked with wavelengths.

FIG. III. 8(a)   THE BEHAVIOUR OF A NEON OPTOGALVANIC SIGNAL WITH DISCHARGE CURRENT
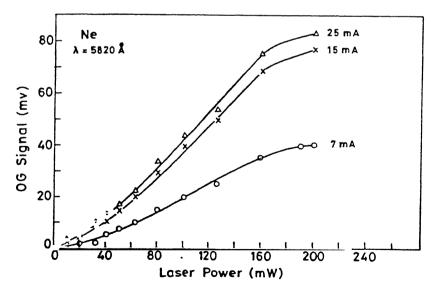


FIG. III. 8(b)   THE SATURATION BEHAVIOUR OF A NEON OPTOGALVANIC SIGNAL WITH LASER POWER
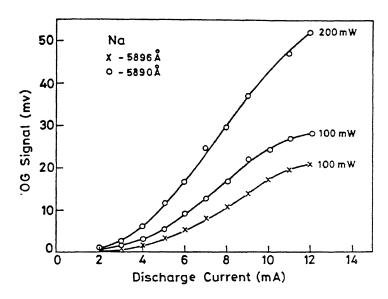
FIG. III. 9(a)   THE BEHAVIOUR OF SODIUM OPTOGALVANIC SIGNALS WITH DISCHARGE CURRENT
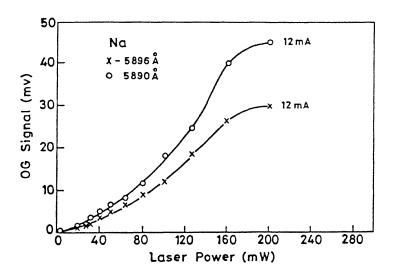


FIG. III. 9(b)   THE SATURATION BEHAVIOUR OF SODIUM OPTOGALVANIC SIGNALS WITH LASER POWER
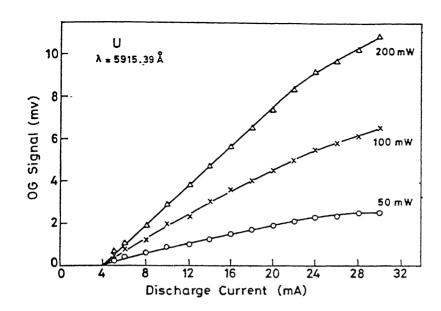
FIG.III.10(a)   THE BEHAVIOUR OF AN URANIUM OPTOGALVANIC SIGNAL WITH

DISCHARGE CURRENT
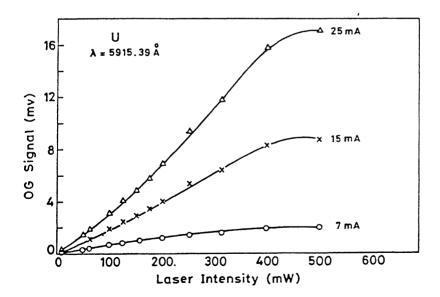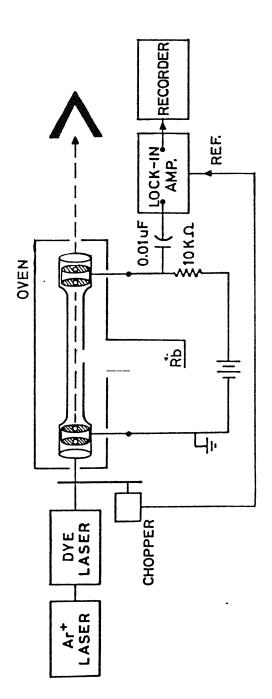


FIG.III.10(b)   THE SATURATION BEHAVIOUR OF AN OPTOGALVANIC   SIGNAL

OF SPUTTERED URANIUM ATOMS WITH LASER POWER

between two stainless steel electrodes was constructed with pyrex glass. It was evacuated to $10^{-6}$Torr and then filled with rubidium and neon at 1.4torr. A stable Rb gas discharge consisting of mainly a positive column was obtained over a current range of 6-9mA at cell temperature $200^{\circ}$C. The experimental arrangement is shown in Fig.III.11. The dye laser beam was chopped at 320Hz to get good signal-to-noise ratio.

OGS of high lying levels (Rydberg states) of Rb has been extensively studied by many authors [20,21] by space charge detection technique. The intermediate levels of Rb were studied here using OGS in a dc discharge. In dc discharge $5^{2}P_{1/2,3/2}$ are well populated by electronic collisions and these atoms are further excited by the laser to higher levels. The recorded OG spectrum is shown in Fig.III.12. All the seven single-photon transitions expected in the range studied and a few two-photon transitions are observed. Cesium impurity present in the rubidium used in the experiment gave Cs spectra in the series $5d^{2}D_{3/2,5/2} \rightarrow nf^{2}F_{5/2,7/2}$ ($11 \leq n \leq 23$). The OG signals of Rb were quite strong; the maximum optogalvanic effect observed was 17% change in the voltage across the discharge tube for 6299.22$\overset{0}{\text{A}}$ transition. The strong background observed in the recorded spectra is due to the direct laser photo-ionization of Rb and Cs.

## III.5.3 IMOGS of Neon

For checking the frequency stability and resolution of the experimental set-up, an experiment using the intermodulated optogalvanic spectroscopy [22] was performed on neon in a
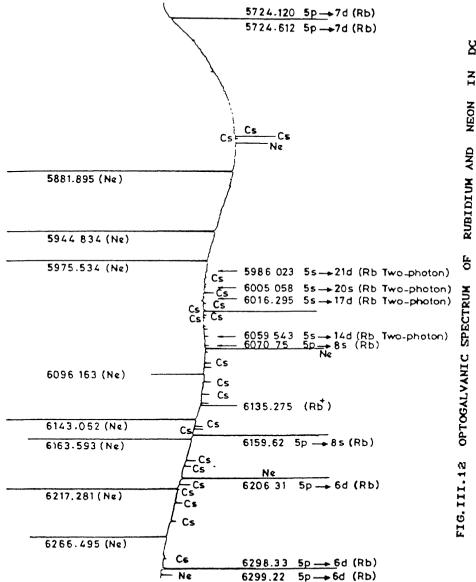
FIG.III.11   THE EXPERIMENTAL SET-UP FOR OPTOGALVANIC   SPECTROSCOPY   OF

RUBIDIUM POSITIVE COLUMN

5724.120  5p → 7d (Rb)
5724.612  5p → 7d (Rb)

Cs ├ Cs ─ Cs
   └ Ne

5881.895 (Ne)

5944 834 (Ne)

5975.534 (Ne)

5986 023  5s → 21d (Rb Two-photon)
Cs
6005 058  5s → 20s (Rb Two-photon)
Cs
6016.295  5s → 17d (Rb Two-photon)
Cs ├ Cs
Cs

6059 543  5s → 14d (Rb Two-photon)
6070 75  5p → 8s (Rb)
Ne

Cs

6096 163 (Ne)

Cs
Cs

6135.275  (Rb⁺)

6143.052 (Ne)       Cs
6163.593 (Ne)

6159.62  5p → 8s (Rb)

Cs
Cs

Ne

Cs       6206 31  5p → 6d (Rb)
6217.281 (Ne)   Cs

Cs

6266.495 (Ne)

Cs       6298.33  5p → 6d (Rb)
Ne       6299.22  5p → 6d (Rb)

FIG.III.12  OPTOGALVANIC  SPECTRUM  OF  RUBIDIUM AND  NEON  IN  DC

DISCHARGE

see-through hollow cathode discharge lamp. The isotope shift between $^{20}$Ne and $^{22}$Ne was measured for 5852Å transition. The measured shift of 2.3GHz confirms the earlier results[23]. The schematic of the experimental set-up and the recorded IMOGS spectrum of neon are shown in Fig.III.13 and Fig.III.14 respectively. The dye laser beam was split into two parts of roughly equal intensity. These beams were chopped at two different frequencies $f_1$(978Hz) and $f_2$(550Hz) and were passed through the hollow cathode discharge lamp in opposite directions. Each beam can saturate the transition separately. When the two beams interact with the same velocity group of atoms nonlinearities are caused and it gives rise to Doppler-free optogalvanic signals at the sum frequencies $(f_1+f_2)$= 1528Hz. The pedestals observed in the spectrum are due to velocity-changing collisions.

## III.6 OGS OF NEODYMIUM

### III.6.1 Introduction

Optogalvanic spectra of neodymium provides the fine structure spectra of both neutral neodymium and singly-ionized neodymium. NdI and NdII which have 4f incomplete shells consist of a large number of both odd and even configurations. This makes the observed fine structure spectra very dense and complex. A large number of energy levels of NdI were identified by many authors[24-28] using traditional spectroscopic techniques. Albertson et.al[29] and Schuurmans[30] gave the first analysis of the NdII spectrum. The assignment of the observed energy levels to various electronic configurations was carried out with the help of

**FIG.III.13    EXPERIMENTAL    SET-UP    FOR    INTERMODULATED    OPTOGALVANIC    SPECTROSCOPY**

FIG. III.14   IMOGS SPECTRUM OF Ne LINE 5852Å
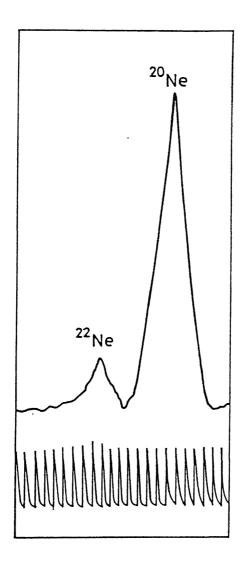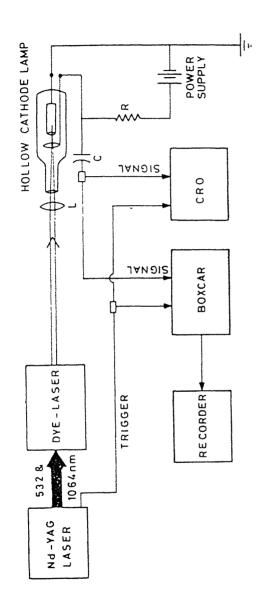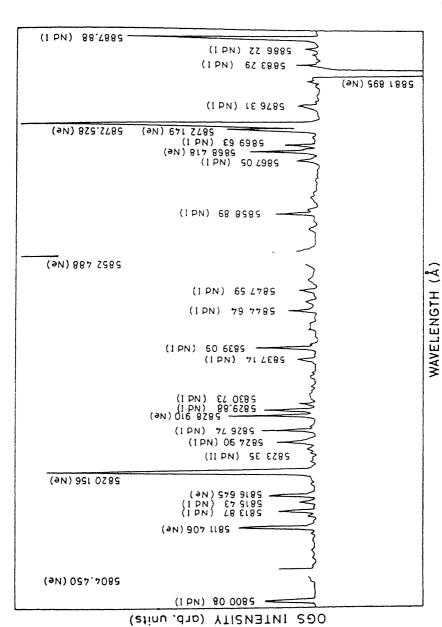
extensive studies of Zeeman effect[31] and isotope shift[32-34]. All the results were critically evaluated and compiled by Martin et.al [35]. A revised interpretation of NdII spectrum was recently provided by Blaise et.al [36] with the help of isotope shift measurements.

The experimental setup used for recording the OGS of neodymium using a cw dye laser was similar to the one given in Fig. II.1. A commercial Nd/Ne hollow cathode lamp (Instrumentations Laboratories Inc.) was operated at 16mA discharge current to produce the atoms and ions of Nd. The dye laser beam was chopped at 440Hz to get the optimum signal-to-noise ratio. The dye laser was scanned over 6400-5710Å wavelength range in all the reproducible scans. For the pulsed OGS, the experimental set-up used is shown in Fig.III.15. A pulsed Rhodamin 6G dye laser was pumped by a Nd-YAG frequency doubler. The OG signals were taken across a ballast resistor of 10kΩ and were fed to a boxcar averager triggered externally from an output of the laser system. The spectra were recorded with 50ns gatewidth and 10$\mu$s time constant settings for the boxcar. The dye laser was scanned over a wavelength range 5800-5530Å using a stepper motor control system. The laser was operated at 50cycle repetition rate with peak powers of about 250kW. Typical OG spectra recorded are shown in Fig.III.16 and Fig.III.17. All the observed neodymium optogalvanic signals were measured with the help of neon calibration lines.

**FIG. III.15  EXPERIMENTAL  ARRANGEMENT  FOR  PULSED  OPTOGALVANIC**

**SPECTROSCOPY**

5887.88 (Nd I)

5886 22 (Nd I)

5883 29 (Nd I)

5881 895 (Ne)

5876 31 (Nd I)

5872.528 (Ne)    5872 149 (Ne)

5869 63 (Nd I)

5868 418 (Ne)

5867 05 (Nd I)

5858 89 (Nd I)

5852 488 (Ne)

5847 59 (Nd I)

5844 64 (Nd I)

5839 09 (Nd I)

5837 14 (Nd I)

5830 73 (Nd I)

5829.88 (Nd I)

5828 910 (Ne)

5826 74 (Nd I)

5824 90 (Nd I)

5823 35 (Nd II)

5820 156 (Ne)

5816 645 (Ne)

5815 43 (Nd I)

5813 87 (Nd I)

5811 406 (Ne)

5804.450 (Ne)

5800 08 (Nd I)

OGS INTENSITY (arb. units)

WAVELENGTH (Å)

FIG.III.16  A TYPICAL CW OPTOGALVANIC SPECTRUM OF NEODYMIUM

## III.8.2 Results and discussion

Lifeng et.al[37] have earlier reported 76 transitions of neodymium using the pulsed OGS. In the present work the optogalvanic spectra of neodymium were recorded in the wavelength range 553-640nm using both CW and pulsed dye lasers. From the observed spectra, 384 spectral lines of NdI and 273 spectral lines of NdII were identified. The tentative classification for most of the observed spectral lines were obtained using the energy levels reported by many authors[35,38]. The strong lines observed in the continuous wave OGS are tabulated in Table1 along with the observed relative intensities. These intensities were not normalized to the dye gain curve but the peak power of the Rhodamine 6G dye laser was kept constant at 160mW in all the reproducible scans. Many new spectral lines were identified in the observed OGS. Wavelength corrections were made for many spectral lines reported by King [24] and Meggers et. al[38].

OGS is an effective detection technique to carry out the atomic spectroscopy of neodymium. Not only the spectra of low-lying levels, but also the spectra corresponding to many high-lying configurations were conveniently recorded using this technique. The signal-to-noise ratio of CW OG spectrum was found to be much better than that of pulsed OG spectrum of neodymium. However, the sinal strengths in pulsed OGS were much bigger showing that the optogalvanic signal of neodymium are not saturated even at 160mW.

Table III.1    Strong spectral lines of Nd observed in the continuous wave OG spectra. Classification and observed relative intensities are provided wherever possible.

| Measured λ(Å) | Species | Transition energy(cm$^{-1}$) odd J-even J | | OGS intensity (arb.units) | Identified λ(Å) | λ (Ref.) |
|---|---|---|---|---|---|---|
| 5729.29 | NdI | 19816 | 5-2366   6 | 19 | 5729.29 | 41 |
| 5731.16 | NdI | 27258 | 3-9814   3 | 3 | - | - |
| 5749.19 | NdI | 25864 | 5-8475   5 | 12 | 5749.19 | 55 |
| 5749.65 | NdI | 17387 | 5-0   4 | 42 | 5749.66 | 55 |
| 5762.o4 | NdI | 29309 | 9-11959   9 | 5 | 5762.08 | 55 |
| 5766.60 | NdI | 31290 | 8-13953   9 | 5 | - | - |
| 5772.15 | NdI | 17319 | 4-0   4 | 13 | 5772.14 | 41 |
| 5776.09 | NdI | 18436 | 4-1128   5 | 21 | 5776.12 | 55 |
| 5780.58 | NdI | 29473 | 5-12178   5 | 1 | 5780.58 | 41 |
| 5784.96 | NdI | 19648 | 7-5048   8 | 22 | 5784.96 | 55 |
| 5788.22 | NdI | 22320 | 7-5048   8 | 9 | 5788.22 | 55 |
| 5788.94 | NdI | 12878 | 4-30148   5 | 4 | - | - |
| 5791.44 | NdI | 12611 | 7-29873   8 | 3 | - | - |
| 5800.07 | NdI | 20918 | 6-3681   7 | 22 | 5800.09 | 55 |
| 5806.41 | NdI | 10004 | 5-27222   4 | 1 | 5806.41 | 41 |
| 5807.70 | NdI | 8800 | 6-26014   6 | 1 | - | - |
| 5810.27 | NdI | 9692 | 7-26898   7 | 1 | - | - |
| 5813.88 | NdI | | - | 16 | 5813.87 | 41 |
| 5815.43 | NdI | 8402 | 7-25593   8 | 7 | 5815.44 | 55 |
| 5818.48 | NdI | 30099 | 5-12917   6 | 1 | - | - |
| 5823.76 | NdI | | - | 3 | 5823.76 | 41 |
| 5824.90 | NdI | 17162 | 5-0   4 | 17 | - | - |
| 5825.85 | NdII | 25876 | 2.5-8716  1.5 | 2 | 5825.87 | 55 |
| 5826.74 | NdI | 20839 | 6-3681   7 | 23 | 5826.84 | 55 |
| 5829.88 | NdI | 26963 | 4-9814   4 | 23 | - | - |
| 5830.73 | NdI | 25621 | 4-8475   5 | 7 | 5830.72 | 55 |
| 5837.14 | NdI | 8402 | 7-25529   8 | 8 | 5837.15 | 41 |
| 5839.09 | NdI | 18249 | 4-1128   5 | 27 | 5837.08 | 41 |
| 5842.87 | NdI | 6854 | 5-23964   6 | 2 | - | - |

| | | | | | | | |
|---|---|---|---|---|---|---|---|
| 5844.74 | NdI | 10160 | 8-27265 | 9 | 12 | 5844.66 | 41 |
| 5845.92 | NdI | 29060 | 9-11959 | 9 | 4 | 5845.95 | 55 |
| 5847.59 | NdI | 10784 | 8-27881 | 9 | 9 | 5847.57 | 55 |
| 5849.60 | NdI | 29008 | 7-11918 | 7 | 2 | 5849.59 | 41 |
| 5851.71 | NdI | 27023 | 7-9939 | 7 | 9 | - | - |
| 5856.68 | NdI | 28179 | 5-11109 | 6 | 3 | 5856.66 | 41 |
| 5858.89 | NdI | 27961 | 8-10897 | 8 | 17 | 5858.91 | 55 |
| 5859.37 | NdI | 19428 | 6-2266 | 6 | 5 | 5859.37 | 41 |
| 5867.06 | NdI | 30993 | 10-13953 | 9 | 10 | 5867.05 | 41 |
| 5868.88 | NdI | 32107 | 10-15073 | 10 | 4 | 5868.70 | 55 |
| 5869.63 | NdI | 17032 | 4-0 | 4 | 14 | - | - |
| 5875.78 | NdI | 27391 | 6-10376 | 5 | 6 | - | - |
| 5876.31 | NdI | 8800 | 6-25813 | 7 | 9 | - | - |
| 5876.96 | NdI | 27785 | 7-17010 | 6 | 1 | - | - |
| 5880.32 | NdI | 25476 | 4-8475 | 5 | 4 | - | - |
| 5883.29 | NdI | 10784 | 8-27777 | 9 | 10 | 5883.29 | 55 |
| 5886.22 | NdI | 29886 | 9-12902 | 8 | 5 | 5886.24 | 55 |
| 5887.18 | NdI | 8402 | 7-25383 | 7 | 1 | 5887.17 | 41 |
| 5887.88 | NdI | 16979 | 3-0 | 4 | 86 | 5887.89 | 41 |
| 5895.56 | NdI | 26072 | 5-9115 | 6 | 3 | 5895.57 | 41 |
| 5895.96 | NdI | 31260 | 10-14304 | 11 | 3 | - | - |
| 5899.49 | NdI | 8800 | 6-25746 | 6 | 7 | 5899.49 | 55 |
| 5900.43 | NdII | 24468 | 3.5-7524 | 3.5 | 3 | 5900.49 | 55 |
| 5905.92 | NdI | 30726 | 8-13798 | 7 | 6 | - | - |
| 5909.85 | NdII | 26274 | 5.5-9357 | 5.5 | 5 | 5909.87 | 55 |
| 5910.63 | NdI | 26029 | 5-9115 | 6 | 3 | 5910.63 | 41 |
| 5914.34 | NdI | 28821 | 8-11918 | 7 | 7 | 5914.40 | 55 |
| 5914.91 | NdI | 18029 | 9-1128 | 5 | 6 | - | - |
| 5919.79 | NdI | 27785 | 7-10838 | 8 | 4 | - | - |
| 5922.80 | NdI | 25354 | 6-8475 | 5 | 1 | - | - |
| 5926.07 | NdI | 14932 | 8-31801 | 7 | 1 | - | - |
| 5927.96 | NdI | 29767 | 7-12902 | 8 | 2 | 5927.94 | 41 |
| 5929.86 | NdI | 27860 | 4-11001 | 3 | 3 | - | - |
| 5931.41 | NdI | 29956 | 9-13101 | 10 | 3 | 5931.43 | 41 |
| 5932.46 | NdI | 30805 | 8-13953 | 9 | 1 | 5832.47 | 41 |
| 5933.33 | NdI | 29767 | 7-12917 | 6 | 1 | - | - |

| | | | | | | | |
|---|---|---|---|---|---|---|---|
| 5935.46 | NdI | 26782 | 8-9939 | 7 | 4 | – | – |
| 5939.73 | NdI | 13799 | 7-30630 | 7 | 3 | 5939.79 | 41 |
| 5941.38 | NdI | 10160 | 8-26987 | 9 | 3 | 5941.39 | 41 |
| 5949.64 | NdI | 25918 | 6-9115 | 6 | 4 | 5949.64 | 55 |
| 5954.53 | NdI | 16844 | 5-33634 | 6 | 2 | – | – |
| 5955.88 | NdI | 19152 | 6-2366 | 6 | 4 | 5955.88 | 41 |
| 5957.63 | NdI | 12611 | 7-29391 | 8 | 1 | – | – |
| 5962.39 | NdI | 28759. | 3-11990 | 2 | 1 | 5962.39 | 41 |
| 5967.87 | NdI | 25227 | 5-8475 | 5 | 2 | 5967.85 | 41 |
| 5968.25 | NdI | 204324 | 6-3681 | 7 | 6 | – | – |
| 5968.66 | NdI | 11108 | 5-27852 | 4 | 1 | – | – |
| 5970.21 | NdI | 13672 | 4-30148 | 5 | 1 | – | – |
| 5977.44 | NdI | 29826 | 10-13101 | 10 | 7 | 5977.42 | 41 |
| 5978.81 | NdI | 25196 | 6-8475 | 5 | 5 | 5978.82 | 41 |
| 5980.87 | NdI | 27716 | 4-11001 | 3 | 1 | – | – |
| 5986.50 | NdI | 27474 | 5-10775 | 6 | 2 | – | – |
| 5990.23 | NdI | 29606 | 7-12917 | 6 | 3 | 5990.21 | 41 |
| 5994.75 | NdI | 27785 | 7-11109 | 6 | 9 | 5994.76 | 55 |
| 5996.45 | NdI | 26611 | 7-9939 | 7 | 7 | 5996.47 | 41 |
| 5996.94 | NdI | 10918 | 5-27589 | 6 | 5 | 5996.95 | 41 |
| 6000.03 | NdI | 17790 | 4-1128 | 5 | 30 | 6000.09 | 41 |
| 6002.51 | NdI | 30608 | 10-13953 | 9 | 4 | 6002.52 | 41 |
| 6006.39 | NdI | 8402 | 7-25046 | 8 | 7 | – | – |
| 6007.65 | NdI | 9692 | 7-26333 | 8 | 29 | 6007.67 | 55 |
| 6020.50 | NdI | 27714 | 7-11109 | 6 | 4 | – | – |
| 6022.63 | NdI | 27374 | 7-10775 | 6 | 6 | 6022.63 | 41 |
| 6023.56 | NdI | 10784 | 8-27381 | 7 | 3 | 6023.56 | 41 |
| 6024.84 | NdI | 8412 | 9-25005 | 7 | 2 | – | – |
| 6025.53 | NdI | 21640 | 7-5048 | 8 | 4 | 6025.54 | 55 |
| 6033.28 | NdI | 30874 | 11-14304 | 11 | 7 | 6033.30 | 41 |
| 6049.84 | NdI | 17652 | 4-1112 | 5 | 14 | – | – |
| 6050.46 | NdI | 30476 | 10-13953 | 9 | 3 | – | – |
| 6052.73 | NdI | 6764 | 6-23281 | 5 | 4 | – | – |
| 6054.48 | NdI | 27998 | 3-11486 | 4 | 3 | 6054.47 | 41 |
| 6061.03 | NdI | 25609 | 6-9115 | 6 | 3 | 6061.05 | 41 |
| 6062.04 | NdI | 12394 | 5-28885 | 5 | 1 | – | – |

| | | | | | | | |
|---|---|---|---|---|---|---|---|
| 6065.16 | NdI | 28661 | 5-12178 | 5 | 3 | – | – |
| 6066.03 | NdI | 29581 | 10-13101 | 10 | 19 | 6063.03 | 55 |
| 6071.07 | NdI | 28426 | 8-11959 | 9 | 1 | – | – |
| 6071.58 | NdI | 28531 | 5-12065 | 5 | – | – | – |
| 6071.70 | NdI | 26842 | 6-10376 | 5 | 14 | 6071.70 | 55 |
| 6075.64 | NdI | 28719 | 4-12264 | 3 | 1 | – | – |
| 6078.43 | NdI | 24922 | 6-8475 | 5 | 1 | – | – |
| 6082.03 | NdI | 20118 | 6-3681 | 7 | 5 | 6082.02 | 41 |
| 6084.59 | NdI | 27328 | 8-10897 | 8 | 8 | 6084.62 | 41 |
| 6086.93 | NdI | 28602 | 6-12178 | 5 | 4 | 6086.94 | 41 |
| 6087.92 | NdI | 6853 | 5-23275 | 4 | 3 | – | – |
| 6101.72 | NdI | 28344 | 9-11959 | 9 | 8 | – | – |
| 6109.10 | NdI | 12394 | 5-28758 | 6 | 2 | – | – |
| 6109.68 | NdI | 21411 | 7-5048 | 8 | 3 | 6109 68 | 41 |
| 6122.13 | NdII | 26206 | 3.5-9877 | 4.5 | 3 | 6122.16 | 41 |
| 6148.56 | NdI | 17387 | 5-1128 | 5 | 8 | 6148.60 | 41 |
| 6149.25 | NdI | 26072 | 5-9814 | 4 | 30 | 6149.28 | 55 |
| 6155.04 | NdI | 28160 | 8-11918 | 7 | 99 | 6155.06 | 55 |
| 6156.92 | NdI | 21286 | 7-5048 | 8 | 4 | 6156.90 | 41 |
| 6161.24 | NdI | 8800 | 6-25026 | 7 | 5 | 6161.26 | 41 |
| 6165.65 | NdI | 26029 | 5-9814 | 4 | 5 | 6165.63 | 41 |
| 6174.29 | NdI | 17319 | 4-1128 | 5 | – | 6174.30 | 41 |
| 6178.18 | NdI | 29980 | 8-13799 | 7 | 2 | – | – |
| 6178.57 | NdI | 30484 | 12-14304 | 11 | 7 | 6178.59 | 55 |
| 6208.22 | NdI | 26878 | 7-10774 | 6 | 5 | 6208.24 | 55 |
| 6218.10 | NdI | 12009 | 5-28086 | 5 | 2 | – | – |
| 6219.69 | NdI | 11887 | 9-27961 | 9 | 1 | – | – |
| 6222.13 | NdI | 26842 | 6-10775 | 6 | 5 | 6222.15 | 41 |
| 6223.38 | NdI | 29165 | 11-13101 | 10 | 22 | 6223.39 | 55 |
| 6226.49 | NdI | 8800 | 6-24856 | 7 | 16 | 6226.50 | 41 |
| 6227.20 | NdI | 9692 | 7-25746 | 6 | 3 | 6227.18 | 41 |
| 6230.21 | NdI | 28311 | 3-12264 | 3 | 2 | – | – |
| 6238.44 | NdII | 24445 | 5.5-8420 | 4.5 | 1 | 6238.50 | 55 |
| 6244.07 | NdI | 27970 | 10-11959 | 9 | 16 | 6244.06 | 41 |
| 6250.43 | NdII | 25352 | 5.5-9357 | 5.5 | 5 | 6250.41 | 41 |
| 6252.78 | NdI | 27474 | 5-11486 | 4 | 3 | – | – |

| | | | | | | | |
|---|---|---|---|---|---|---|---|
| 6258.71 | NdII | 26640 | 3.5-10666 | 3.5 | 22 | 6258.74 | 41 |
| 6260.64 | NdI | 26345 | 5-10376 | 5 | 4 | – | – |
| 6263.29 | NdI | 26963 | 4-11001 | 3 | 3 | 6263.23 | 41 |
| 6269.41 | NdI | 25885 | 7-9939 | 7 | 3 | – | – |
| 6278.94 | NdI | 31756 | 9-15834 | 9 | 3 | – | – |
| 6279.39 | NdI | 30608 | 10-14688 | 9 | 9 | – | – |
| 6284.04 | NdI | 15220 | 6-31129 | 5 | 1 | – | – |
| 6285.78 | NdI | 27961 | 8-12056 | 7 | 8 | 6285.79 | 55 |
| 6288.00 | NdI | 15899 | 3-0 | 4 | 3 | 6288.03 | 41 |
| 6291.44 | NdI | 18256 | 7-15890 | 4 | 4 | – | – |
| 6297.05 | NdI | 27835 | 10-11959 | 9 | 12 | – | – |
| 6302.21 | NdI | 15863 | 6-0 | 4 | 7 | 6302.20 | 41 |
| 6307.01 | NdI | 6764 | 6-22615 | 7 | 6 | 6307.02 | 41 |
| 6308.25 | NdI | 27913 | 6-12065 | 5 | 7 | 6308.26 | 55 |
| 6310.47 | NdI | 26740 | 9-10897 | 8 | 29 | 6310.49 | 55 |
| 6314.77 | NdI | 12927 | 7-28758 | 6 | 1 | – | – |
| 6321.22 | NdI | 8402 | 7-24217 | 7 | 4 | 6321.22 | 55 |
| 6324.98 | NdI | 24218 | 7-8012 | 6 | 4 | 6324.99 | 41 |
| 6331.88 | NdI | 30476 | 10-14688 | 9 | 5 | 6331.87 | 41 |
| 6363.94 | NdI | 26484 | 5-10774 | 6 | 5 | 6363.94 | 41 |

# REFERENCES

1. R.B.Green, R.A.Keller, G.G.Luther, P.K.Schenck and J.C.Travis, Appl. Phys.Lett.29, 727(1976).

2. W.B.Bridges, J.Opt.Soc.Am. 68,352(1948).

3. J.B.M.Goldsmith and J.E.Lawler, Contemp. Phys.22 ,235(1981).

4. P.Camus(ed) Proc.Int. colloquium on optogalvanic spectroscopy and its Applications, Aussois, J.de physique C7-44(1983).

5. P.D.Foote and F.L.Mohler, Phys.Rev.26, 195(1925).

6. F.M.Penning, Z.Physik.46, 355(1928).

7. M.M.Joshi,Nature 154,147(1944).

8. C.Kenty,Phy.Rev.80, 95(1950).

9. K.W.Meissner and W.F.Miller,Phys.Rev.92, 896(1953).

10. R.A.Keller, B.E.Warner, E.F.Zalewski, P.Dyer, R.Engleman,Jr. and B.A.Palmer, J.de Physique C7-44,23(1983).

11. D.M.Pepper IEEE J.Quant.Electron QE-14 , 971(1978).

12. M.Maeda, Y.Nomiyama and Y.Miyazoe, Opt.comm.39 ,64(1981).

13. D.K.Doughty and J.E.Lawler, Phys.Rev. A 28,773(1983).

14. H.B.Valentini, Opt.Comm.53,313(1985).

15. G.Erez, S.Lavi and E.Miron, IEEE J.Quantum Electron QE-15,1328(1979).

16. G.N.Rao,J.Govindarajan and M.N.Reddy, Hyp. Int.38, 539(1987).

17. P.Hannaford, Contemp. Phys. 24, 251(1983).

18. A.R.Striganov and N.S.Sventitskii,"Tables of Spectral Lines of Neutral and Ionized Atoms"(IFI/Plenum,NY 1968).

19. R.A.Keller,R.Engleman,Jr., and E.F.Zalewski, J.Opt.Soc.Am. 69,738(1979).

20. K.C.Harvey and B.P.Stoicheff,Phys.Rev.Lett.38,537(1977).

21. B.P.Stoicheff and E.Weinberger, Can.J.Phys.57,2143 (1979).

22. J.E.Lawler, A.I.Ferguson, J.E.M.Goldsmith, D.J.Jackson and A.L.Schawlow, Phys. Rev. Lett. 42, 1046(1979).

23. D.R.Lyons, A.L.Schawlow and G.-Y Yan, Opt.Comm.38, 35(1981).

24. A.S.King, Astrophysics. J. 78, 9(1933).

25. F.W.Paul, Phys. Rev. 49. 156(1936).

26. G.E.M.A.Hassan and P.F.A.Klinkenberg, Physica, 29,1133 (1963).

27. J.Blaise, J.Chevillard, J.verges and J.F.Wyart, Spectrochim Acta 25B, 333(1970).

28. C.Morillon, Spectrochim Acta 25B, 513(1970).

29. W.E.Albertson, G.R.Harrison, and J.R.McNally,Jr. Phys.Rev. 61, 167(1942).

30. PH.Schuurmans, Physica 11, 419(1946).

31. J.Blaise, J.F.Wyart, R.Hoekstra and P.J.G. Kruiver, J.Opt.Soc.Am. 61, 1335(1971).

32. G.Noldeke, Z.Physik 143, 274(1955).

33. S.A.Ahmad, and G.D.Saksena, Physica 85C, 191(1977).

34. S.A.Ahmad and G.D.Saksena, Spectrochim Acta 38B, 1065(1983).

35. W.C.Martin, R.Zalubas, and L.Hagan, Atomic Energy levels, The Rare Earth Elements, Nat. Bur.Stand. (U.S) 60 , 422(1978).

36. J.Blaise, J-F. Wyart, M.T.Djerad and Z.B.Ahmad, Physica Scripta 29, 119 (1984).

37. Y.Lifeng, J.Chunkyang, Z.Guiyan and C.Junwen, Chin, Phys. 4,219(1984).

38. W.S.Meggers, C.H. Corliss and B.F.Scribner eds."Tables of Spectral Lines Intensities, Arranged by Elements" (U.S. Govt. Printing Office,Washington,1975).

# FINE AND HYPERFINE STRUCTURE STUDIES OF LUTETIUM

## IV.1 INTRODUCTION

Even though lutetium is a rare-earth element it behaves more like a 5d group element with fully filled 4f-shell rather than a rare-earth element. Infact LuI is structurally one of the simplest spectrum of the 5d group and differ much from the spectra of other rare earth elements. The atomic spectrum of neutral lutetium was first investigated through arc and spark emission by Meggers and Scribner[1] in 1930. This early investigation led to the discovery of the $5d6s^2$ $^2D$ ground term. King[2] in 1931 determined the classification for 108 lines covering 2951-6463Å range. Later, many authors[3-5] have extended the energy level scheme and assigned configurations to many levels measured using several techniques. Zeeman-effect studies[6,7] and the measurement of the hfs of spectrallines[8] in the visible region also contributed to the classification of the measured energy levels. The study of infrared spectrum of LuI in the range $2692-10082cm^{-1}$ by Fourier transform spectroscopy by Verges and Wyart[9] and parametric study of the hyperfine constants of several configurations by Wyart[10] have further extended the analysis of LuI.

Lutetium has two stable natural isotopes $^{175}Lu$(97.4%) and $^{176}Lu$(2.6%) with nuclear spins 7/2 and 7 respectively. Hyperfine structure constants for the ground state doublet $^2D_{3/2,5/2}$ of

[175]Lu were measured accurately by Figger and Wolber[11] using Atomic Beam Magnetic Resonance(ABMR). Several authors[12-14] have studied the hyperfine structure and isotope shift of [175]Lu and [176]Lu for some excited states by means of optical spectroscopy. Blaise et al[12] have studied the hfs of some low lying levels of LuI and LuII using Fabry-Perot interferometer and deduced the value of the nuclear spin of [176]Lu as I=7. However there are still quite a few energy levels lying above $25000cm^{-1}$ and belonging mainly to $6s^2np$ , $6s^2nd$ , $6s^2nf$ and $5d6s7s$ configurations yet to be studied to understand more about these high lying configurations. These levels can be reached by multi-step processes to investigate the hyperfine structure using the sensitive spectroscopic techniques for detectoin.

In this thesis laser optogalvanic spectroscopic technique was employed to study the fine and the hyperfine structure spectra of many low as well as high lying configurations of lutetium in $5650-6250\overset{o}{A}$ wavelength range. The relative intensities of the observed spectral lines in the OGS were measured. The classification for some of the new transitions of LuI are provided. Using a single frequency dye laser as the excitation source in the optogalvanic detection set-up, the hyperfine structure of many excited levels of [175]Lu were investigated and the corresponding hyperfine coupling constants were measured. The hyperfine structure of the three high-lying configurations $5d6s7s$, $6s^27d$ and $6s^225p$ have also been possible to study by LOGS technique.
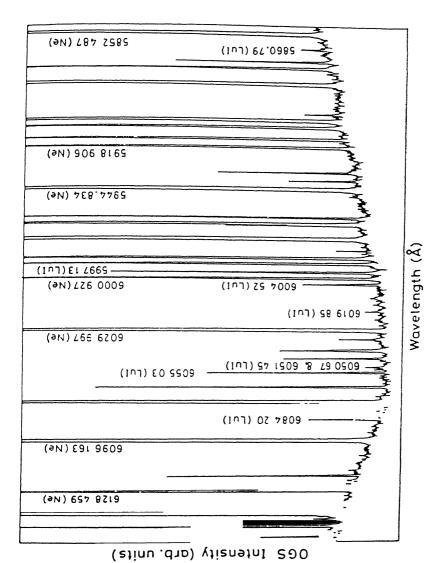
## IV.2 OPTOGALVANIC SPECTROSCOPY OF LUTETIUM

Optogalvanic spectroscopy of lutetium was carried out using an experimental set-up similar to the one shown in Fig.III.1. A commercial(Hamamatsu) lutetium hollow cathode discharge lamp with neon as a buffer gas was used in the experiment. The lamp provided a stable discharge at 15mA current and populated appreciably the ground state and many of the excited metastable states of lutetium. The excitation laser beam was modulated at 430Hz and the optogalvanic signals were recorded as voltage changes across a 40kΩ ballast resistor. The dye laser was scanned over a wavelengh range 5650-6250Å and 16 transitions of LuI were recorded in the OGS spectrum.
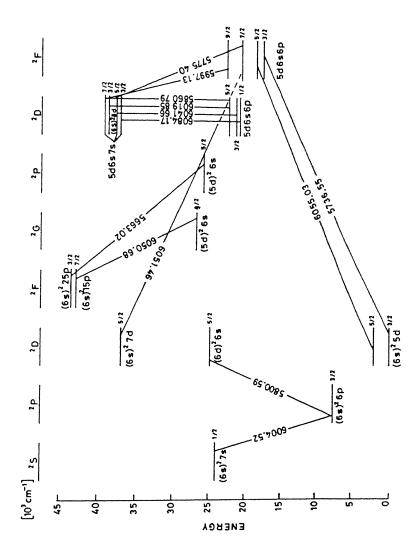
A typical optogalvanic spectrum of lutetium is shown in Fig.IV.1. The strong neon lines observed in the OG spectrum were used for the wavelength calibratiion of the recorded spectrum. The simplified energy level diagram of LuI is shown in Fig.IV.2 and the observed transitions are pointed out in the figure.

## IV.3 HYPERFINE STRUCTURE OF $^{175}$Lu

The experimental set-up for high-resolution OGS was similar to the one shown in Fig.III.2. A frequency stabilized single frequency ring dye laser was used to excite the transitions and scan the frequency over 30GHz to record the hyperfine structure patterns of many transitions in $^{175}$LuI spectrum. In the recorded Doppler limited high resolution OGS spectra the hyperfine structure patterns of $^{175}$Lu were fairly well resolved because the hypefine splittings of the energy levels of $^{175}$Lu are usually

**Fig.IV.1** Typical OGS spectrum of lutetium Neon lines used for wavelength calibration are identified along with the lutetium lines.

Fig.IV.2 The simplified energy level scheme of lutetium. All the observed lutetium transitions are indicated.

larger than the Doppler broadening of the sputtered lutetium atoms. Doppler broadening of the sputtered lutetium atoms in the hollow cathode lamp at the operating current was found to be about 740MHz whereas the hyperfine splittings are typically more than 1000MHz.

Since $^{176}$Lu isotope has very low natural abundance (2.6%) the signals corresponding to it will not show up in the observed spectra, unless one goes for very high sensitivities of the detection and maintains at the same time good signal-to-noise ratio. Typical hfs spectra of $^{175}$Lu recorded using LOGS , computer fitted and theoretically generated hfs spectra and the hyperfine level schemes with expected relative intensities are given in various figures starting from Fig. IV.3 to Fig. IV.14.

## IV.4 RESULTS AND DISCUSSION

All the observed lutetium transitions are listed in Table IV.1 along with their measured relative OGS intensities. The intensities of the observed lines were not normalized to the dye gain curve but the peak power of the laser was fixed at 130mW in all the reproducible scans. Many new transitions of lutetium were observed in the OGS at the wavelengths 5663.02, 5793.25, 5830.0, 5842.5, 6019.85, 6050.68, 6051.46 and 6084.17Å and the classification for some of these transitions is provided using the known energy levels[18]. All the possible dipole transitions are worked out using a computer program with the input data of both odd and even energy levels and angular momenta.

Measurement of the hyperfine structure splittings of the atomic states enables us to determine the hyperfine structure

Table IV.1. Spectral lines of LuI observed in OGS along with the observed relative intensities. The uncertainities in the measurement of the wavelengths are about $\mp 0.1 \overset{o}{A}$.

| Wavelength $(\overset{o}{A})$ | Transition | Energy($cm^{-1}$) lower level — upper level | observed intensity | Ref. $(\lambda)$ |
|---|---|---|---|---|
| 5663.02 | $5d^2 6s\ ^4P_{5/2}$ $-6s^2 25p\ ^2P_{3/2}$ | 25860.76-43514.29 | - | - |
| 5736.55 | $5d6s^2\ ^2D_{3/2}$ $-5d6s6p\ ^4F_{3/2}$ | 0.00-17427.28 | 12 | 17 |
| 5775.40 | $5d6s6p\ ^4F_{7/2}$ $-5d6s7s\ ^4D_{5/2}$ | 20432.53-37742.56 | 180 | 17 |
| 5793.25 | - | - | 12 | - |
| 5800.59 | $6s^2 6p\ ^2P_{3/2}$ $-5d^2 6s\ ^2D_{5/2}$ | 7476.35-24711.19 | 18 | 17 |
| 5830.0 | - | - | 20 | - |
| 5842.5 | - | - | 10 | - |
| 5860.79 | $5d6s6p\ ^4D_{5/2}$ $-5d6s7s\ ^4D_{7/2}$ | 22221.64-39279.48 | 12 | 17 |
| 5997.13 | $5d6s6p\ ^4F_{9/2}$ $-5d6s7s\ ^4D_{7/2}$ | 22609.46-39279.48 | 144 | 17 |
| 6004.52 | $6s^2 6p\ ^2P_{3/2}$ $-6s^2 7s\ ^2S_{1/2}$ | 7476.35-24125.86 | 34 | 17 |
| 6019.85 | $5d6s6p\ ^4D_{5/2}$ $-6s^2 8d\ ^4D_{5/2}$ | 22221.64-38828.77 | 8 | - |
| 6041.66 | $5d6s6p\ ^4D_{3/2}$ $-5d6s7s\ ^4D_{5/2}$ | 21195.37-37742.56 | - | 17 |
| 6050.68 | $5d^2 6s\ ^2G_{9/2}$ $-6s^2 15f\ ^2F_{7/2}$ | 26671.32-43193.85 | 9 | - |
| 6051.46 | $5d6s6p\ ^4F_{7/2}$ $-6s^2 7d\ ^2D_{5/2}$ | 20432.53-36952.93 | 5 | - |
| 6055.03 | $5d6s^2\ ^2D_{5/2}$ $-5d6s6p\ ^4F_{5/2}$ | 1993.92-18504.56 | 78 | 17 |
| 6084.17 | $5d6s6p\ ^4D_{1/2}$ $-5d6s7s\ ^4D_{3/2}$ | 20762.42-37193.98 | 32 | - |

$\lambda$ wavelength
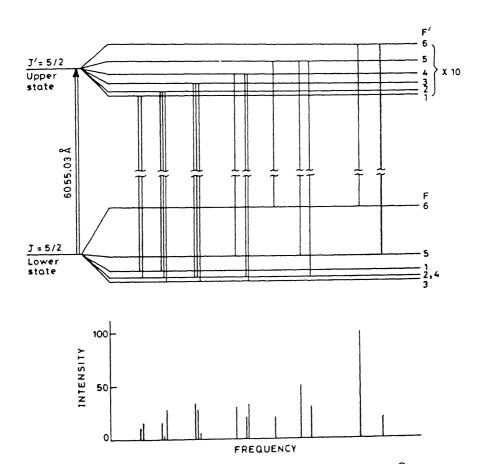
Fig. IV.3  The hfs level scheme of LuI line $\lambda = 6055.03\text{Å}$. Thereotical intensity ratios for the hfs components are given at the bottom of the figure.

Fig. IV.4 Recorded hfs spectrum of LuI line $\lambda = 6055.03\text{Å}$. Vertical bars indicate the positions of hyperfine components and their length proportional to the theoretically expected relative intesities. The components are identified by F quantum numbers from lower-state to upper-state.

Fig.IV.5 Fitted hfs spectrum of LuI line λ=6055.03Å.
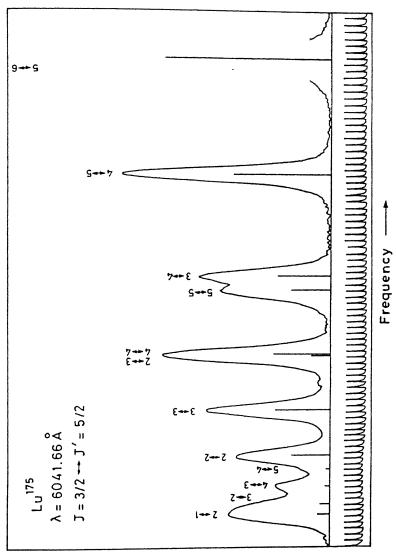
Fig. IV.8   The hfs level scheme of LuI line λ=6041.66Å. Theoretical intensity ratios for the hfs components are given at the bottom of the figure.
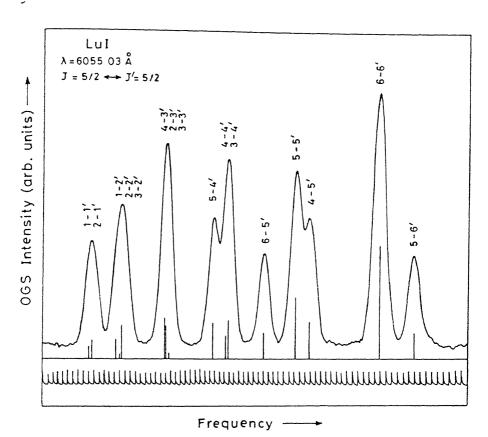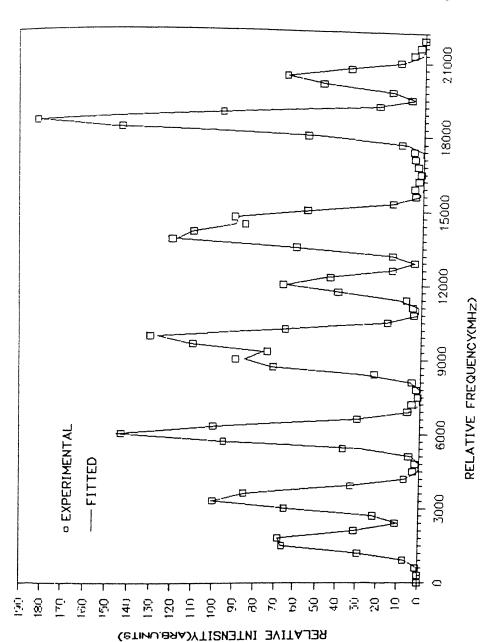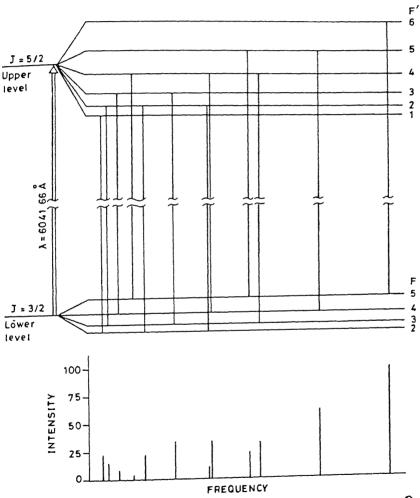
Fig.IV.7  Recorded hfs spectrum of LuI line λ=6041.66Å.
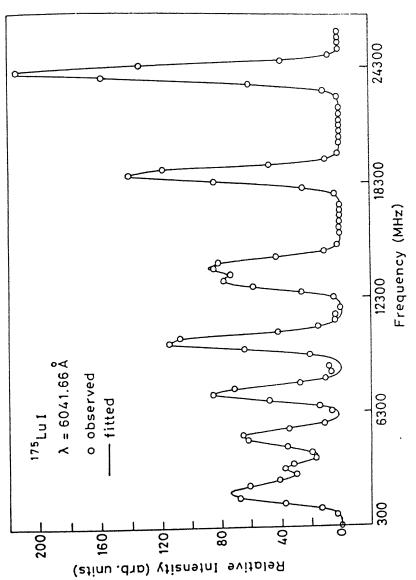
Fig.IV.8  Fitted hfs spectrum of LuI line λ=6041.66Å.
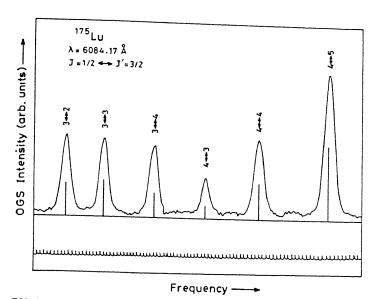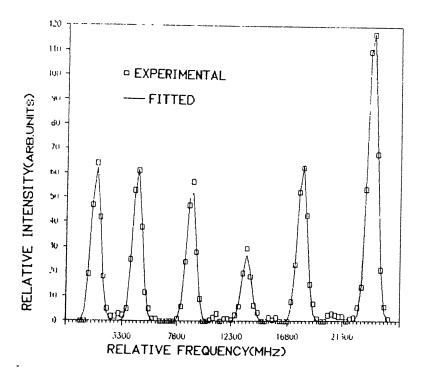
Fig.IV.9(a)   Recorded hfs spectrum of LuI line $\lambda$=6084.17Å.
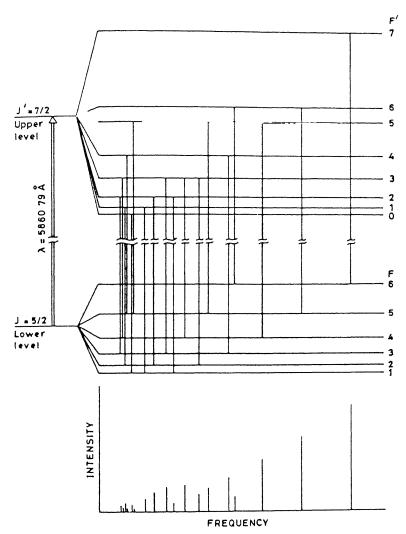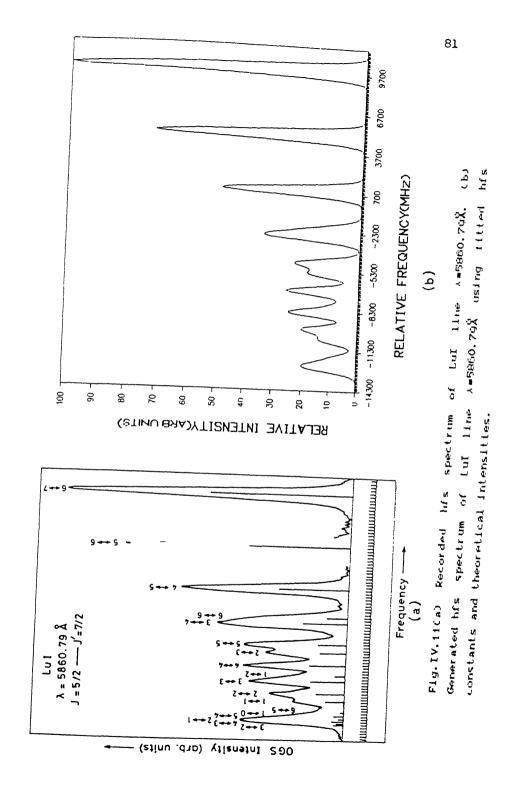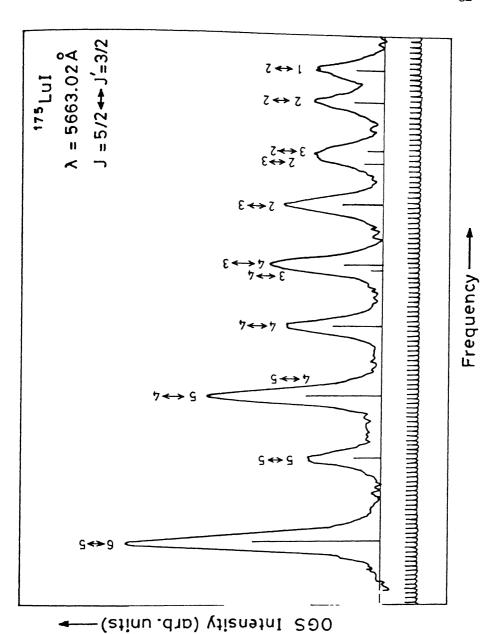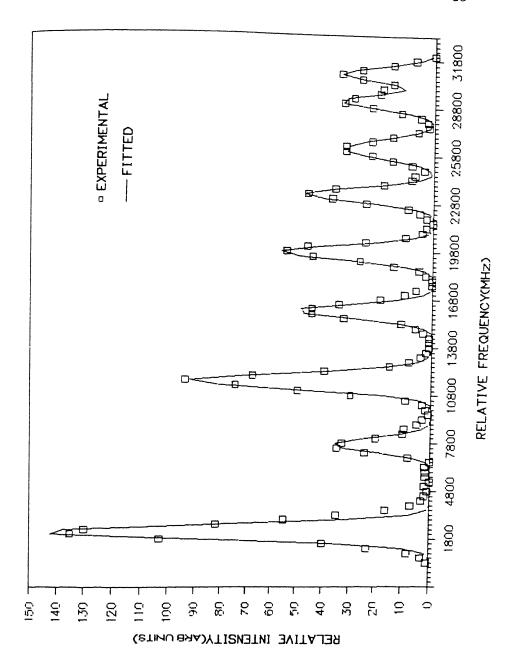
Fig. IV.10    The   hfs   level   scheme   of   LuI   line   $\lambda = 5860.79 \overset{\circ}{A}$. Theoretical intensity ratios for the hfs components are   given   at the bottom of the figure.

Fig.IV.11(a) Recorded hfs spectrum of LuI line λ=5860.79Å. (b) Generated hfs spectrum of LuI line λ=5860.79Å using fitted hfs constants and theoretical intensities.

Fig.IV.12  Recorded hfs spectrum of LuI line λ=5663.02Å.

Fig.IV.13  Fitted hfs spectrum of LuI line λ=5663.02Å.

Fig.IV.14  Saturation of hfs components with laser power. The  hfs
components of LuI line λ=6041.68Å are presented.

coupling constants for the states. These constants as detailed in chapter II are further expressed in terms of hfs-parameters which in turn give valuable information about nuclear structure and the electronic wave functions near the nucleus. As seen from the recorded spectra, the hyperfine spectra of $^{175}$Lu deviates considerably from the interval rule because of the large nuclear electric quadrupole moment Q=5.68b. In fact, the hfs level schemes for some of the states do not follow any order, for example the hfs level scheme of 6055.03Å spectral line shown in Fig.IV.3. For the same reason the assignment of the observed peaks and thus the analysis are very complicated.
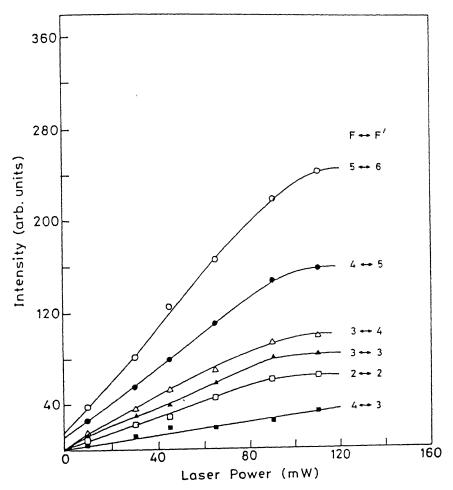
The analysis of the recorded hfs spectra was carried out using a systematic procedure as follows. In most of the recorded hfs spectra atleast a few of the strong hfs components(diagonal) can be identified by comparing the intensities of the observed peaks with the relative intensities calculated for various hfs components. The theoretical relative intensities were tabulated by Kopferman[19] for different nuclear spin values for the transitions between the angular momentum states J=1/2 to J=13/2. Then the hyperfine coupling constants for both the lower and the upper levels of a transition were deduced as preliminary estimates from the observed spectra by measuring the spacings between suitable pairs of hyperfine components and using the Casimir formula(2.25)

$$E = \frac{hA}{2} K + \frac{hB}{4} \frac{(3/2)K(K+1)-2I(I+1)J(J+1)}{I(2I-1)J(2J-1)}$$

where $K = F(F+1)-I(I+1)-J(J+1)$ and $F = (I+J),(I+J-1),\ldots\ldots,\mid I-J\mid$.

For splittings of a single fine structure level, the Casimir formula reduces to

$$\Delta\nu_{12} = A \frac{K_1 - K_2}{2} + \frac{3B \ [K_1(K_1+1) - K_2(K_2+1)]}{8IJ \ (2J-1) \ (2I-1)}$$  (4.1)

In the observed hfs spectra, the relative peak spacings were measured with respect to the 300MHz frequency markers which were recorded simultaneously with the hfs spectra

Since the broadening of the spectral lines in hollow cathode discharges is predominantly due to the Doppler broadening each hfs component in the hfs spectra recorded can be considered as a pure Gaussian profile with the halfwidth equal to Doppler width. Hence with approximate initial guess values, each of the spectra was fitted to a function $F(x)$ which is essentially a summation of n (n is the number of hfs components) Gaussian profiles with equal halfwidths.

$$F(x) = \sum_n I_n \ \exp\left[ -(x-x_n)^2/0.36 \ \delta x_D^2 \right]$$  (4.2)

where $I_n$ is the intensity of the $n^{th}$ hfs component and $\delta x_D$ is the half width of the Gaussian profile. The other input data required for this fitting procedure are peak heights $I_n$, peak width(FWHM) $\delta x_D$, $J_{lower}$, and $J_{upper}$ . Besides A, B, A$'$, B$'$ the peak heights $I_n$ and the peak width $\delta x_D$ were also kept as free parameters . The peak heights of the individual hfs components were manually obtained from the observed spectra for well resolved components. However the approximate intensities of the unresolved hfs components were determined by normalizing their calculated intensities with the observed intensities of the well resolved

components.

The computer program which does the minimization of sum of the square errors at all the given experimental points also takes care of the nonlinearities in the observed intensities of individual hfs components. In this algorthm the independent variables can be fixed with lower and upper bounds. This enables us to reduce the total number of variable parameters by fixing the known parameters to improve the fitting. Most often the best fitted values of the hfs constants of the excited states were computed by fixing the accurate values for the hfs constants of the lower levels. The analyses of the hfs spectra could be duly verified by generating the hfs spectra of the transitions using the hyperfine coupling constants obtained by computer fits and the theoretically calculated intensities and then comparing them with the observed spectra.

The errors associated in the fitted parameters A, B, A′ and B′ depend on many factors. They depend primarily on the type and quality of the recorded spectrum and secondarily on the quality of the fit. In most of the recorded OGS spectra the noise level was found to be much lower than one part in hundred. To decide the quality of the fit several self-evaluatory logics were incorporated in the algorithm. It not only monitors the ranges of each one of the independent variables but also cautions about the variables lying out of the ranges. The fit is generally considerd good for its lowest sum of the squares of the deviations and IFAIL equal to zero. For evaluating the uncertainities in the fitted hfs coupling constants one first estimates the probable total errors

in the measurement of the data points. Later the level of uncertainity in each one of the fitted parameters is decided from the $\chi^2$ plots with the changes in the value of each fitted parameters.

The intensities of the individual components of a hyperfine spectrum in OGS often deviate from classical intensities due to saturation effects[15]. A simple sum rule is usually inadequate to specify the actual relative intensities of the hfs components. However, at lower laser powers, the observed intensities of various hfs components are in close agreement with classical intensities. In Fig.IV.14, the saturation behaviour of some hfs components of $\lambda=6041.66\text{Å}$ transition is given. It is apparent from Fig.IV.14 that the weaker components of the hfs spectrum saturate at higher laser powers compared with the stronger hfs components and thus responsible for the nonlinearities observed in the OGS signals at higher laser powers. The hyperfine coupling constants of the states studied are tabulated in Table IV.2. Our LOGS data are in good agreement, within our experimental accuracy, with the data reported by others by means of other experimental methods. Theoretically calculated values for $22609.46\text{cm}^{-1}$ level is in agreement with our measured values. However the calculated values[10] for $7476.35\text{cm}^{-1}$ and $20432.53\text{cm}^{-1}$ states and the earlier reported values[9] for $25860.76\text{cm}^{-1}$ state are not in agreement with our data and comparisions are given in the table IV.2. The A and B values for the multiplet of 5d6s7s configuration and for the levels $6s^2 7d\ ^2D_{5/2}$ and $6s^2 25p\ ^2P_{3/2}$ are given here for the first time. The uncertainities in present measurements are usually about

Table IV.2. Hyperfine coupling constants of $^{175}$LuI determined by LOGS. The numbers in parentheses are uncertainities in units of the last figure.

| Excitation energy (cm$^{-1}$) | J parity | This work(LOGS) A | B | Other work A | B | Ref. |
|---|---|---|---|---|---|---|
| 0.00 | 3/2$^+$ | 195.6(40) | 1506(15) | 194.332921 | 1511.396267 | 11 |
| 1993.92 | 5/2$^+$ | 149.0(60) | 1862(18) | 146.776472 | 1860.656132 | 11 |
| 7476.35 | 3/2$^-$ | 220.8(80) | 2091(23) | 222.9(90) | 2111.7(450) | 12 |
| 17427.28 | 3/2$^-$ | -915.8(60) | 1759(22) | -924.7(5) | 1767(6) | 13 |
| 18504.56 | 5/2$^-$ | 989.6(40) | 1100(20) | 987.2(4) | 1117(6) | 14 |
| 20432.53 | 7/2$^-$ | 1016.5(40) | 2531(22) | 1068$^c$(48) | 2316$^c$(111) | 10 |
| 20762.42 | 1/2$^-$ | -2250.8(40) | - | -2244(3) | - | 9 |
| 21195.37 | 3/2$^-$ | 1025.9(50) | 615(14) | 1020(15) | 600(120) | 9 |
| 22221.64 | 5/2$^-$ | 1095.5(90) | 813(25) | 1092(3) | 855(30) | 9 |
| 22609.46 | 9/2$^-$ | 1079.0(90) | 3838(17) | 1077$^c$(48) | 3801$^c$(111) | 10 |
| 24125.86 | 1/2$^+$ | 1758.3(110) | - | 1770(3) | - | 12 |
| 24711.19 | 5/2$^+$ | 901.9(50) | -43(20) | 883.5(45) | -42(60) | 9 |
| 25860.76 | 5/2$^+$ | 886.2(60) | 341(22) | 1116(15) | 360(60) | 9 |
| 36952.93 | 5/2$^+$ | 184.3(60) | 116(28) | - | - | - |
| 37193.98 | 3/2$^+$ | 1108.9(50) | 142(16) | - | - | - |
| 37742.56 | 5/2$^+$ | 1725.1(50) | 961(20) | - | - | - |
| 39279.48 | 7/2$^+$ | 1570.9(90) | 2090(24) | - | - | - |
| 43514.29 | 3/2$^+$ | -734.1(50) | -261(22) | - | - | - |

$^c$ calculated value

5MHz for A values and 20Mhz for B values. However, the uncertainities were estimated for each of the measurement separately and given in the parentheses with the corresponding values. The numbers in the parentheses represent the possible deviations in units of the last recorded digits.

Hyperfine structure pattern of each of 5793.25Å and 5830.0Å lines contain seven well resolved peaks whereas the hfs patterns of 5842.5 and 6019.85Å lines contain five and nine well resolved peaks respectively in Dopper limited recordings. The hfs spectra of 5793.25Å and 6019.85Å lines show that these lines could be classified with ΔJ=0 transitions. However the hfs spectra of all these unclssified lines require a reinvestigation preferably using a Doppler-free technique so that an unambiguous classification for these spectral lines may be possible.

## IV.5 CONCLUSIONS

LOGS is a useful, convenient and sensitive technique for studying both fine and hyperfine specrta of high lying configurations of LuI using hollow cathode discharge lamps. Classification to several new transitions to 5d6s7s, $6s^2 7d$ and $6s^2 25p$ are provided. The present hyperfine structure data are not only valuable for the classification of the levels but would also be useful to obtain the radial parameters of the different atomic electrons in lutetium which in turn enable us to estimate the different contributions to the hyperfine Hamiltonian.

# REFERENCES

1. W.F.Meggers, and B.F.Scribner, J.Res.Nat.Bur. stand. 5, 73(1930).

2. A.S.King Astrophys.J.74, 328(1931).

3. P.F.A.Klinkenberg, Physica 21, 53(1954).

4. P.Camus, and F.S.Tomkins, J. de Physique 33,197(1972).

5. L.F.H.Bovey, E.B.M.Steers and H.S.Wise, A.E.R.E.R-3225(1960).

6. J.Anderson, Ph.D.Thesis,London Univ. (1956).

7. E.H.Pinnington, Can. J.Phys.41,1294,1305(1963).

8. U.Horstmann, G.Noldeke and A.Steudel, Ann. Physik 12,14(1964)

9. J.Verges and J.-F.Wyart, Physica Scripta 17,495(1978).

10. J.-F.Wyart, Physica Scripta 18,87(1978).

11. H.Figger and G.Wolber, Z.Physik 264,95(1973).

12. J.Blaise, J.Bauche, S.Gerstenkorn, and F.S.Tomkins, J.Phys. Radium 22,417(1961).

13. D.Zimmermann,P.Zimmermann,G.Aepfelbach and A.Kuhnert,Z.Physik A295, 307(1980).

14. A.Nunnemann,D.Zimmermann and P.Zimmermann Z.physik A 290, 123(1979).

15. G.N.Rao, J.Govindarajan and M.N.Reddy, Hyp.Int. 38, 539(1987).

16. R.Engleman, Jr., R.A.Keller and C.M.Miller, J. Opt. Soc. Am.B,2, 897(1985).

17. Tables of Spectral Line Intensities, Arranged by Elements. W.F.Meggers, C.H.Corliss, and B.F.Scribner, eds. (U.S.Government Printing Office, Washington,1975).

18. Atomic Energy Levels, The Rare Earth Elements, W.C.Martin, R.Zalubas, and L.Hagan, eds.(U.S.Government Printing Office, Washington, 1978).

# CHAPTER V

## FINE AND HYPERFINE STRUCTURE STUDIES OF HOLMIUM

### V.1. INTRODUCTION

Unlike lutetium, holmium is a rare-earth element with unfilled 4f-shell and has quite complex spectra. The first understanding of the spectrum of neutral holmium was due to the extensive studies done by Blaise et al[1,2] in 1972 and Wyart et al[3] in 1973. Spector[4] studied holmium spectrum in the near infrared($0.759-1.2\mu$m) and assigned 460 lines to HoI or HoII. But the analysis of the HoI spectrum was really further extended by the elaborate work carried out by Wyart, Camus and Verges[5] in 1977 and by Wyart and Camus[6] in 1978. Wyart et al[5] have studied the infrared spectrum of holmium in the range $2493-12344$cm$^{-1}$ using Fourier transform spectroscopy and classified as many as 913 spectral lines between 144 odd and 116 even levels of HoI. This study also yeilded the hyperfine structure constants for 111 odd and 66 levels of 9 different configurations. Wyart and Camus[6] have interpreted the energy levels of neutral holmium by means of parametric studies of groups of configurations and determined the hfs constants for many odd and even levels using the calculated eigen functions.

Hyperfine structure of the electronic ground state $4f^{11}6s^2 \, {}^4I_{15/2}$ has been measured precisely by Dankwort et al[7] in 1974 using ABMR technique. Recently Burghardt et al[8] and Childs

et al.[9] have measured the hfs constants of the remaining states of the ground multiplet to a high precision using ABMR technique combined with a state-selective laser-induced detection of the resonant atoms and laser-rf double-resonance technique respectively. Childs et al[9] have also measured the hfs constants of the several excited levels to give new and unambiguous classifications. However the classification of many states of the high-lying configurations is not yet verified by the hfs measurements. This limitation was mainly due to the weak thermal population of the higher lying states in atomic beam magnetic resonance experiments.

In this thesis the fine structure spectra of many low-lying as well as high-lying configurations of holmium were studied in 5660-6200Å wavelength range using LOGS in a hollow cathode discharge. The observed relative intensities for many of the identified strong HoI transitions were measured. Classification for many of the new transitions of HoI are provided. Using a single frequency dye laser as the excitation source, the hyperfine structure of many low as well as high lying levels were investigated and the hyperfine structure coupling constants of the levels were extracted.

## V.2 OPTOGALVANIC SPECTROSCOPY OF HOLMIUM

Optogalvanic spectroscopy of holmium was recorded using a similar experimental set-up as shown in Fig.III.1. A commercial(Hamamatsu) holmium hollow cathode discharge lamp with neon buffer gas was used in the experiment. At 15mA of operating

current the hollow cathode lamp provides a stable dicharge and populates appreciably the ground and many excited matastable states. The excitation laser beam was chopped at 430Hz and the optogalvanic signals were recorded by a lock-in detection. A 40kΩ ballast resistor was used to optimize the experimental parameters. The dye laser was scanned over a wavelength range 5650-6200Å and recorded the OGS spectra of holmium which is highly reproducible.

A part of the recorded OGS spectrum of holmium is shown in Fig.V.1. The neon lines which were used for calbrating the wavelengh of the recorded spectrum and some of the strong holmium lines are identified in the figure. The graph is linear in wavelengh to the first order.

## V.3  HYPERFINE STRUCTURE OF $^{165}$Ho

The experimental set-up used for recording the hyperfine structure of holmium is very similar to the one shown in Fig.III.2. A frequency stabilized single frequency ring dye laser was used to excite the transitions of HoI and scan the frequency of the laser over 30GHz to record the hyperfine structure of several transitions of $^{165}$Ho. The stable isotope of holmium $^{165}$Ho with nuclear spin I=7/2 has large nuclear magnetic moment $\mu_I$=+4.125$\mu_N$ and a quadrupole moment Q=+2.64b. Therefore the hyperfine structure of HoI lines are usually very broad and often spread over more than 30GHz. The hfs components for most of the HoI spectral lines get well resolved in the Doppler-limited spectra because the energy separations among the hyperfine transitions are usually larger than the Doppler broadening of the

sputtered holmium atoms. The Doppler broadening which is the major broadenig of the spectral lines of the sputtered holmium atoms in the hollow cathode discharge was estimated to be typically 830MHz at the operating current.

The typical hfs spectra of $^{165}$Ho recorded using LOGS, computer fitted and theoretically generated hfs spectra and the hfs level schemes with theoretically calculated relative intensities are given in various figures starting from Fig.V.2 to Fig.V.12.

## V.4 RESULTS AND DISCUSSION

The optogalvanic spectrum of holmium contains about 29 lines of HoI in the scan range of 5650-6200Å. Out of the observed 29 lines 12 of them are observed for the first time. Most of these new lines are identified as the transitions from the intermediate states to the high-lying states belonging to the even configuration $4f^{11}6s7p$ . All the identified transitions are listed in Table V.1 along with the observed relative OGS intensities. Classification is provided to many of the observed new lines using the known energy levels of HoI. The intensities of the observed spectral lines were not normalized to the lasing dye gain curve but the peak power of the dye laser was fixed at 145mW in all the scans which are quite reproducible.

All the recorded hfs spectra of $^{165}$Ho were analysed by the same procedure as explained in the previous chapter [section IV.4]. Even though the contribution from the quadrupole interaction in holmium is significant, it is easy to identify the

Table V.1 OGS spectra of HoI along with the observed relative intensities. Classifications of the lines are provided wherever possible.

| Wavelength (Å) | Source | J | Transition | J' | Observed intensity | Ref. (λ) |
|---|---|---|---|---|---|---|
| 5659.58 | HoI | 6.5 | 9147.08-26811.32 | 7.5 | - | 11 |
| 5674.70 | HoI | 9.5 | 9741.50-27358.81 | 10.5 | 38 | 11 |
| 5691.47 | HoI | 10.5 | 11322.31-28887.78 | 10.5 | 20 | 11 |
| 5696.57 | HoI | 8.5 | 20315.89-37865.77 | 7.5 | 11 | 11 |
| 5708.07 | HoI | 7.5 | 19276.94-36791.24 | 8.5 | 9 | - |
| 5720.22 | HoI | 6.5 | 18867.40-36344.52 | 7.5 | 20 | - |
| 5730.89 | HoI | 7.5 | 21069.22-38513.79 | 6.5 | 5 | - |
| 5734.02 | HoI | 5.5 | 8605.16-26039.99 | 4.5 | 12 | 11 |
| 5737.8 | HoI | | - | | 17 | - |
| 5738.85 | HoI | 5.5 | 20060.76-37481.94 | 6.5 | 21 | - |
| 5749.58 | HoI | 7.5 | 19276.94-36663.94 | 7.5 | 11 | - |
| 5751.24 | HoI | 6.5 | 9147.08-26529.83 | 5.5 | 13 | - |
| 5751.56 | HoI | 6.5 | 20241.31-37623.09 | 7.5 | 25 | - |
| 5757.18 | HoI | 6.5 | 20258.27-37623.09 | 7.5 | 23 | - |
| 5790.67 | HoI | 9.5 | 20124.25-37388.72 | 8.5 | 11 | - |
| 5821.90 | HoI | 9.5 | 11689.77-28861.41 | 8.5 | 8 | 11 |
| 5860.28 | HoI | 7.5 | 0.00-17059.35 | 6.5 | 22 | 11 |
| 5882.99 | HoI | 6.5 | 5419.70-22413.14 | 5.5 | 10 | 11 |
| 5892.56 | HoI | 5.5 | 8605.16-25571.15 | 6.5 | - | 11 |
| 5921.76 | HoI | 7.5 | 0.00-16882.31 | 7.5 | 24 | 11 |
| 5948.03 | HOI | 6.5 | 5419.70-22227.34 | 7.5 | - | 11 |

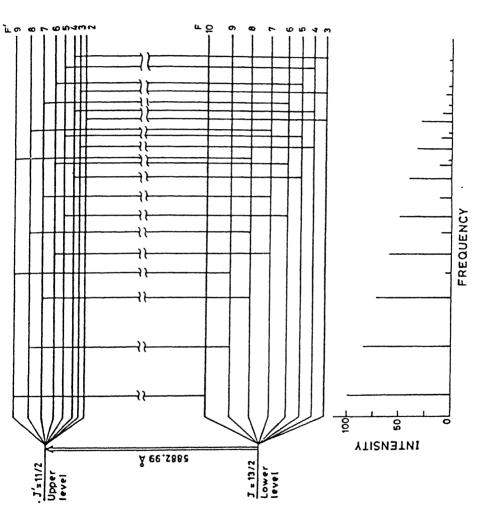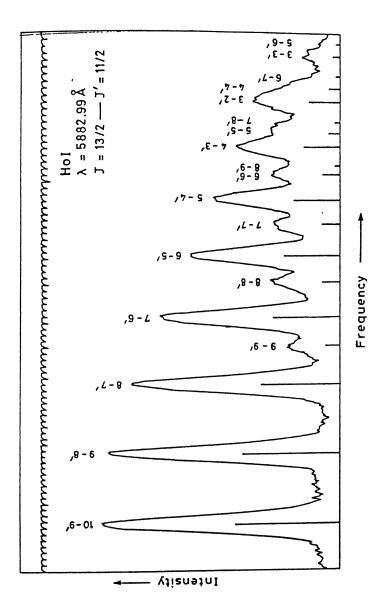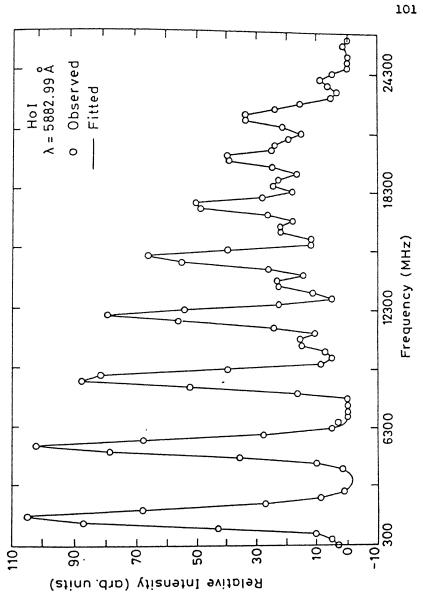| | | | | | | |
|---|---|---|---|---|---|---|
| 5972.76 | HoI | 6.5 | 5419.70-22157.86 | 6.5 | – | 11 |
| 5973.52 | HoI | 7.5 | 0.00-16735.95 | 6.5 | – | 11 |
| 5982.90 | HoI | 7.5 | 0.00-16709.82 | 8.5 | 75 | 11 |
| 5999.79 | HoI | 8.5 | 15130.31-31793.06 | 8.5 | – | – |
| 6021.27 | HoI | 5.5 | 20060.76-36663.94 | 6.5 | – | 11 |
| 6021.56 | HoI | 9.5 | 20124.25-36726.65 | 9.5 | – | 11 |
| 6081.77 | HoI | 7.5 | 0.00-16438.03 | 8.5 | 20 | 11 |
| 6133.60 | HoI | 8.5 | 8378.91-24678.25 | 9.5 | 12 | 11 |

Fig.V.2 The hfs level scheme of HoI line λ=5882.99Å. Thereotical intensity ratios for the hfs components are given at the bottom of the figure.

Fig.V.3 Recorded hfs spectrum of HoI line λ=5882.99Å. Vertical bars indicate the positions of hyperfine components and their length proportional to the theoretically expected relative intensities. The components are identified by F quantum numbers from lower-state to upper-state.
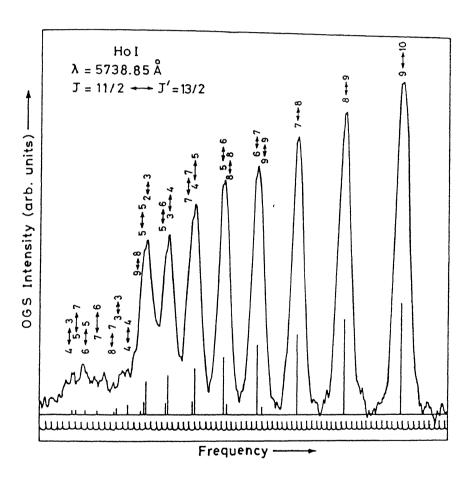
Fig. V. 4 Fitted hfs spectrum of HoI line λ=5882.99Å.

Fig. V.5   Recorded hfs spectrum of HoI line λ=5738.85Å.

Fig. V.8  Fitted hfs spectrum of HoI line λ=5738.85Å.

Fig.V.7 Recorded hfs spectrum of HoI line λ=5674.70Å. All but the first two weak hfs components are present in the figure.
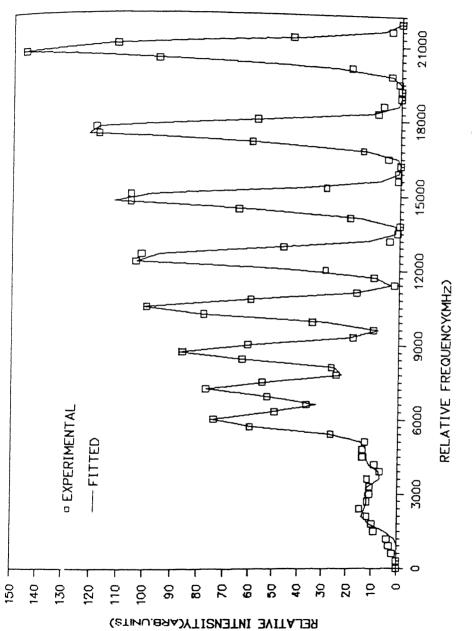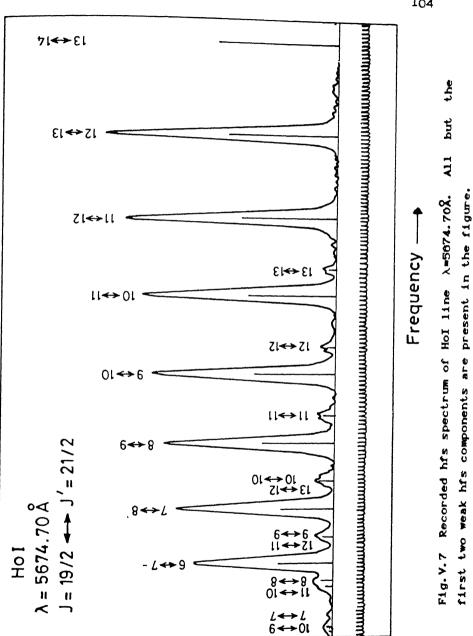
Fig. V. 8  Generated hfs spectrum of HoI line λ=5874.70Å  using  the
fitted hfs constants and the calculated intensities.

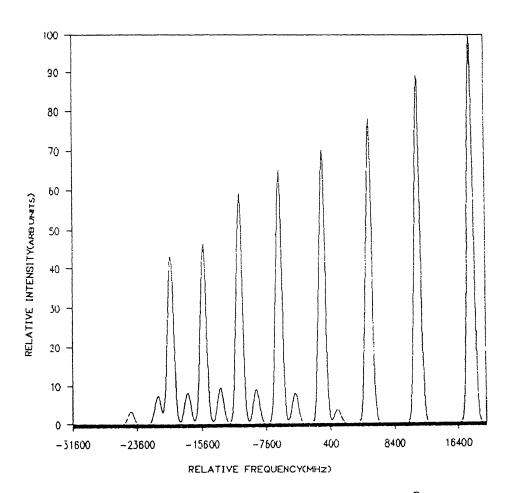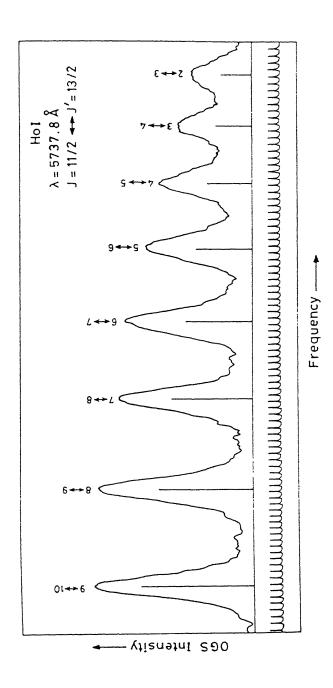Fig.V.9  Recorded hfs spectrum of HoI line λ=5737.8Å. Only the strong diagonal hfs components are identified in the spectrum.
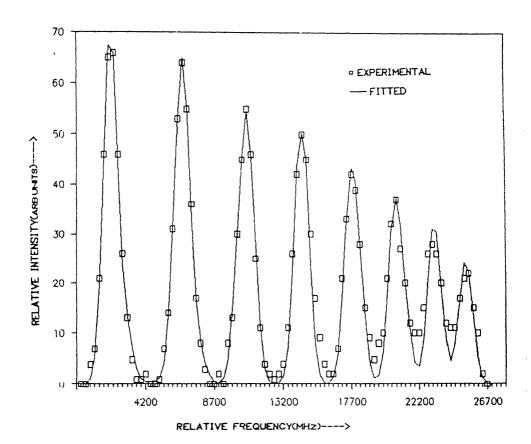
Fig. V.10  Fitted hfs spectrum of HoI line λ=5737.8Å.

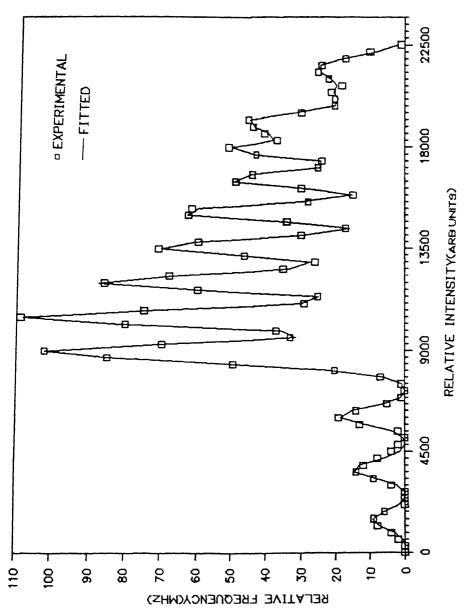Fig. V.11   Recorded hfs spectrum of HoI line λ=5972.76Å.

Fig.V.12  Fitted hfs spectrum of HoI line λ=5972.76Å.

diagonal hfs components. Infact many of the hfs spectra of HoI consist of many well resolved hfs components in the Doppler-limited recording. The fittings were initially performed only for the well resolved single component peaks to estimate the better values of the calculated hfs constants. However the entire hfs spectrum was fitted using the normalized intensities of individual hfs components and the fitted hfs constants. The excitation laser power was always maintained at lower lavel($\simeq$55mW) to avoid the saturation effects which are normally responsible for the nonlinearitis in the intensities of the individual hfs components.

The recorded and fitted hfs spectra of HoI line $\lambda$=5882.99Å are shown in Fig.V.3 and Fig.V.4 respectively. In this spectrum 14 of the 16 hfs components are well resolved and hence the spectrum was well fitted. The hfs constants of the upper levels of 6021.56, 6021.27, 5790.67, 5757.18, 5751.56, 5749.58, 5738.85, 5730.89, 5720.22, 5708.07 and 5696.57Å transitions were determined for the first time. The ambiguty in the classification of 37865.77cm$^{-1}$ level was removed by confirming J=15/2 from the study of the hfs spectrum of $\lambda$=5696.57Å line and the classification of 36663.94cm$^{-1}$ level was corrected by assigning J=15/2 from the study of the hfs spectrum of $\lambda$=5749.58Å line. The correct wavelength as well as the classification for the unclssified line 5739.24Å[11] have been provided using the present studies. A strong signal due to the transition originating from 20060.76cm$^{-1}$ was detected at the wavelength $\lambda$=5738.85Å and no signal was detected at the wavelength $\lambda$=5739.24Å. The recorded hfs spectrum of $\lambda$=5738.85Å is shown in

Fig.V.6. The hfs spectrum of another fairly strong unclssified line at 5737.8Å was recorded and its pattern suggests that it must be a transition of ΔJ=+1. The recorded and the fitted hfs spectra are given in Fig.V.9 and Fig.V.10 respectively. The analysis of the hfs spectrum was done with the classification J=11/2<—>J′=13/2 for which the observed relative intensities of the hfs components match well with the expected intensities. The hyperfine coupling constants for both lower and upper levels of this spectral line were estimated from the fit and they are

$$A=644.5(60) \qquad B=-1358(18)$$
$$A′=90.8(70) \qquad B′=-890(22)$$

The observed hfs spectra of 5734.02, 5973.52 and 5999.79Å look very similar and are highly overlapping. The calculated hfs constants for the upper levels of 5734.02 and 5973.52Å transitions are found inaccurate as the generated hfs spectra using these hyperfine coupling constants do not match well with the observed spectra. Hence it will be of value to perform this experiment with a Dopper-free method so that accurate values for the hfs constants of these levels may be obtained.

The hyperfine coupling constants of the states studied are tabulated in Table V.2. Our LOGS data are in good agreement, within our experimental accuracy, with the data reported by others by means of other experimental methods.

Table V.2  Hyperfine coupling constants of $^{165}$HoI  determined by LOGS.
Numbers in parentheses are uncertainities in units of the last figure.

| Excitation energy ($cm^{-1}$) | J Parity | hfs constants(MHz) | | | | Ref. |
|---|---|---|---|---|---|---|
| | | This work(LOGS) | | Other work | | |
| | | A | B | A | B | |
| 0.00 | 15/2$^-$ | 801.5(40) | -1667(12) | 800.58309 | -1668.089 | 8 |
| 5419.70 | 13/2$^-$ | 940.5(40) | -1222(19) | 942.0(30) | -1230(300) | 5 |
| 8378.91 | 17/2$^+$ | 784.7(60) | 601(23) | 776.4(45) | 606(300) | 5 |
| 8605.16 | 11/2$^-$ | 1039.9(50) | -1052(16) | 1034.6(5) | -1051(7) | 9 |
| 9147.08 | 13/2$^+$ | 912.0(60) | 2659(20) | 916.6(5) | 2668(7) | 9 |
| 9741.50 | 17/2$^+$ | 740.1(70) | 1672(28) | 743.4(45) | 1680(300) | 5 |
| 11322.31 | 21/2$^+$ | 711.3(90) | 3360(31) | 693.9(45) | 3318(300) | 5 |
| 11689.77 | 19/2$^+$ | 756.1(70) | 2606(24) | 732.6(30) | 2970(150) | 5 |
| 16438.03 | 17/2$^+$ | 816.9(50) | 2040(18) | 819.7(5) | 2035(20) | 9 |
| 16709.82 | 17/2$^+$ | 1137.9(60) | -1806(20) | 1138.8(15) | -1806(60) | 5 |
| 16882.31 | 15/2$^+$ | 480.6(50) | -716(19) | 477.7(5) | -675(20) | 9 |
| 17059.35 | 13/2$^+$ | 557.0(50) | -981(21) | 557.1(30) | -978(150) | 5 |
| 18867.40 | 13/2$^-$ | 1478.3(70) | -478(25) | 1481.7(15) | -474(60) | 5 |
| 19276.94 | 15/2$^-$ | 1298.7(70) | -1881(27) | 1302.0(15) | -1884(60) | 5 |
| 20060.76 | 11/2$^-$ | 553.4(40) | -544(16) | 549.6(15) | -549(60) | 5 |
| 20124.25 | 19/2$^-$ | 920.2(40) | -783(19) | 922.4(15) | -789(60) | 5 |
| 20241.31 | 13/2$^+$ | 1092.6(50) | 429(17) | 996.3(30) | 345(150) | 5 |
| 20258.27 | 13/2$^+$ | 1424.6(50) | 1902(22) | 1427.7(30) | 1890(150) | 5 |
| 20315.89 | 17/2$^-$ | 612.4(60) | -1310(27) | 616.2(15) | -1305(60) | 5 |
| 21069.22 | 15/2$^-$ | 424.1(60) | -1851(20) | 426.0(15) | -1860(60) | 5 |
| 22157.86 | 13/2$^+$ | 732.6(40) | 222(14) | 743.4(30) | 228(150) | 5 |

| | | | | | | |
|---|---|---|---|---|---|---|
| 22227.36 | 15/2$^+$ | 1318.8(60) | −2068(27) | 1308.6(5) | −2122(20) | 9 |
| 22413.14 | 11/2$^+$ | 617.7(50) | −661(15) | 618.9(15) | −666(60) | 5 |
| 24678.25 | 19/2$^-$ | 1215.6(70) | −1057(24) | 1212.3(30) | −1035(150) | 5 |
| 25571.15 | 13/2$^+$ | 1412.1(60) | −1275(22) | 1407.15(3) | −1290(21) | 8 |
| 26529.83 | 11/2$^-$ | 751.0(60) | 1895(20) | 752.7(30) | 1890(150) | 5 |
| 26811.32 | 15/2$^-$ | 1326.7(60) | 588(19) | 1320.3(30) | 585(150) | 5 |
| 27358.81 | 21/2$^-$ | 1161.1(80) | 1896(29) | 1164.0(30) | 1890(150) | 5 |
| 28861.41 | 17/2$^-$ | 634.0(60) | 201(19) | 618.3(30) | −180(150) | 5 |
| 28887.78 | 21/2$^-$ | 905.7(70) | 1388(31) | 956.7(30) | 1590(150) | 5 |
| 36344.52 | 15/2$^+$ | 1997.6(70) | −284(20) | − | − | − |
| 36663.94 | 13/2$^+$ | 850.0(80) | 1340(23) | − | − | − |
| 36726.65 | 19/2$^+$ | 1305.2(70) | −617(32) | − | − | − |
| 36791.24 | 17/2$^+$ | 1620.0(80) | 1615(28) | − | − | − |
| 37388.72 | 17/2$^+$ | 1188.5(70) | −262(22) | − | − | − |
| 37481.94 | 13/2$^+$ | 778.0(60) | 639(31) | − | − | − |
| 37623.09 | 15/2$^-$ | 720.5(50) | 919(20) | − | − | − |
| 37865.77 | 15/2$^+$ | 1094.7(70) | −2744(34) | − | − | − |
| 38513.12 | 13/2$^+$ | 225.1(60) | −2018(28) | − | − | − |

## V.5 CONCLUSIONS

LOGS is a sensitive technique for studying the weak transitions of HoI in hollow cathode discharge. Since the Doppler broadening of the spectral lines of sputtered holmium atoms in hollow cathode discharges is small the hyperfine structure of the high-lying levels in holmium can be studied quite efficiently. In this thesis, the hyperfine structure of many excited states including nine states belonging to $4f^{11}6s7p$ high-lying even configuration of HoI were investigated using this technique quite efficiently. The present experimental data particularly the hfs constants determined for the levels of $4f^{11}6s7p$ configuration are valuable for evaluating the radial parameters of the electrons.

## REFERENCES

1. J.Blaise, P.Camus, G.Guelachvili, J.Verges, and J.F.Wyart, C.R.Acd.Sci.Ser.B274, 1302(1972).

2. J.Blaise, P.Camus, G.Guelachvili, J.Verges, and J.F.Wyart, C.R.Acd.Sci.Ser.B275, 81(1972).

3. J.F.Wyart, J.Blaise, J.Verges, P.Camus and M.Fred, "Recent progress in the analysis of the arc spectrum of holmium," presented at the Fifth Congress of the Euoropean Group for Atomic Spectroscopy, Lund, Sweden,1983.

4. N.Spector,Phys.Scr. 9, 313(1974).

5. J.Wyart, P.Camus and J.Verges, Physica 92C, 377(1977).

6. J.Wyart, and P.Camus, Physica 93C, 227(1978).

7. W.Dankwort, J.Ferch,and H.Gebauer, Z.Phys. 267, 229(1974).

8. B.Burgardt, S.Buttgenbach, N.Glaeser, R.Harzer, G.Meisel, B.Roski and F.Traber, Z.Phys.A307, 193(1982).

9. W.J.Childs, David R.Cok, and L.S.Goodman, J.Opt.Soc.Am. 73, 151(1983).

10. Atomic Energy Levels, The Rare Earth Elements, W.C.Martin, R.Zalubas, and L.Hagan,eds.(U.S.Governament Printing Office, Washington,1978).

11. Tables of Spectral Line Intensities, Arranged by Elements. W.F.Meggers, C.H.Corliss, and B.F.Scribner, eds.(U.S.Government Printing Office, Washington, 1975).

CHAPTER VI


FINE AND HYPERFINE STRUCTURE STUDIES OF PRASEODYMIUM


VI.1. INTRODUCTION

Praseodymium is a typical rare-earth element with an unfilled 4f-shell constituting $4f^3 6s^2$ as the ground state configuration. It has a number of configurations of both parities even below $10000 cm^{-1}$ and leads to a vast number of allowed transitions. Furthermore, the configuration mixing in high-lying configurations adds much to the complication of classifying the dense spectra of PrI and PrII. The line list of PrI and PrII was initially given by King[1] in 1928, and later by Zalubas and Wilson[2] in 1965, and Zalubas and Borchardt[3] in 1973 with the help of emission and absorption spectra. But much of the progress in the classification of levels has been due to the vast studies made by Blaise, Verges, Wyart, Camus and Zalubus[4]. The National Bureau of Standards published the listing of the lines with the classification wherever available in 1975[5], and the listing of the known energy levels in 1978[6].

Praseodymium has only one stable isotope with nuclear spin I=5/2. The hyperfine structure (hfs) of the ground multiplet has been studied to a high precision by Lew [7] in 1953 and Bokelen etal [8] in 1975 using the atomic-beam magnetic-resonance technique. Ramsey[9] measured the hfs of the ground state to extremely high precision using Ramsey separated field technique.

The hyperfine structure of $4f^2 5d6s^2$ and $4f^2 5d^2 6s$ configurations has been studied by Ginibre[10] using Fourier transform spectroscopy and provided many new levels of these configurations. Childs and Goodman[11] reported the hfs constants for 15 lower levels and 34 higher levels using high-resolution laser-rf double resonance technique on an atomic beam of Pr. However the hfs of vast number of the energy levels belonging to the various high lying mixed configurations is not yet known which would have helped considerably to understand these configurations better.

In this thesis the fine structure spectra of many odd and even configurations of praseodymium were studied in 5760-6250Å wavelength range using LOGS in a hollow cathode discharge. The observed relative intensities for all the identified strong PrI and PrII transitions were measured[12]. Classification for many of the new transitions of PrI are provided. Using a single frequency dye laser as the excitation source, the hyperfine structure of many low as well as high lying levels were recorded and the hyperfine structure constants of the levels involved have been measured.

## VI.2 OPTOGALVANIC SPECTROSCOPY OF PRASEODYMIUM

Optogalvanic spectroscopy of praseodymium was carried out using an experimental set-up similar to that shown in Fig.III.1. A commercial (Instrumentation Laboratory Inc.) praseodymium hollow cathode discharge lamp with neon as a buffer gas was used in the experiment. At 16mA of operating current the hollow cathode lamp provided a stable discharge and populated appreciably the ground

and many excited matastable states. The excitation laser beam was chopped at 440Hz and recorded the optogalvanic signals by a lock-in detection. A 40kΩ ballast resistor was used in the discharge circuit for optimum optogalvanic signals and discharge noise. The dye laser was scanned over a wavelength range 5760-6250Å and the dense and highly reproducible OGS spectra of praseodymium were recorded.

A typical OGS spectrum of praseodymium is shown in Fig.VI.1. The neon lines which were used for calibrating the wavelengh of the recorded spectrum and some of the praseodymium lines are identified in the figure. The graph is linear in wavelengh to the first order.

## VI.3 HYPERFINE STRUCTURE OF $^{141}$Pr

The experimental set-up for high resolution OGS of Pr is similar to the one shown in Fig.III.2. A frequency stabilized single frequency ring dye laser was used to excite the transitions of PrI and scan the frequency of the laser over 30GHz to record the hyperfine structure of many transitions of $^{141}$Pr. Though the hyperfine structure patterns of $^{141}$Pr were not resolved so well as in the case of lutetium and holmium in the Doppler limited OGS, all the diagonal($\Delta F = \Delta J$) hfs components get well resolved because the energy separations among the hyperfine transitions involved in a particular atomic transition of PrI are usually larger than the Doppler broadening of the sputtered praseodymium atoms. The Doppler broadening of the sputtered praseodymium atoms in the hollow cathode discharge at operating current was estimated to be
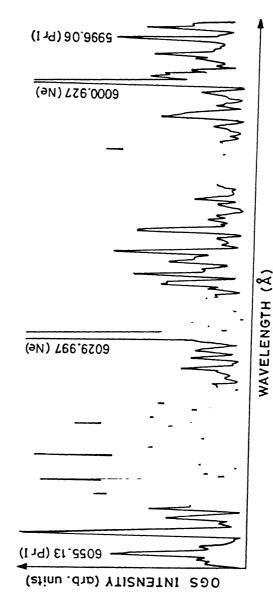
Fig.VI.1 Typical OGS spectrum of praseodymium. Neon lines used for wavelength calibration are identified along with some praseodymium lines.

typically 850MHz.

The isotope $^{141}$Pr has a large nuclear magnetic dipole moment $\mu_I=+4.275\mu_n$ and very small nuclear electric quadrupole moment $Q_I=-0.06b$. Hence the magnetic interaction is a predominent factor in the hyperfine interaction of Pr while the quadrupole interaction is almost negligible. Thus the observed hfs spectra of $^{141}$Pr usually follow the flag pattern owing to the validity of Landé interval rule. The typical hfs spectra of $^{141}$Pr recorded using LOGS, computer fitted and theoretically generated hfs spectra and the hfs level schemes with theoretically calculated relative intensities are given in various figures starting from Fig.VI.2 to Fig.VI.11.

## VI.4 RESULTS AND DISCUSSION

The optogalvanic spectrum of Pr is very rich and contains 299 lines of Pr in the scan range 5760-6250Å. Out of the observed 299 lines 85 strong lines were identified with PrI transitions and 43 strong lines with PrII transitions. All the identified transitions are listed in Table IV.1 along with the measured relative OGS intensities. Classification is provided to 38 of the newly observed transitions using the known energy levels[6,11] of PrI. The intensities of the observed spectral lines were not normalized to the lasing dye gain curve but the peak power of the dye laser was fixed at 130mW in all the scans which are highly reproducible.

All the recorded hfs spectra of $^{141}$Pr were analysed in the same way as it is detailed in section IV.4. It is simpler in PrI to identify the strong diagonal hfs components. The preliminary

Table VI.1  OGS  spectra of PrI and  PrII  along  with  the observed  relative intensities.  Classifications of the lines  are provided wherever possible. The uncertainities in the  measurement of wavelengths are about ±0.3Å

| Wavelength (Å) | Source | J | Transition | J | Observed intensity | Ref. (λ) |
|---|---|---|---|---|---|---|
| 5710.95 | PrI | 8.5 | 9770-27275 | 8.5 | - | 13 |
| 5729.02 | PrI | 6.5 | 6603-24053 | 6.5 | - | 13 |
| 5739.28 | PrI | 6.5 | 6603-24022 | 5.5 | - | 13 |
| 5744.92 | PrI | 5.5 | 6714-24116 | 6.5 | - | - |
| 5769.79 | PrII | 6 | 9647-26973 | 5 | 21.6 | 5 |
| 5779.28 | PrI | 8.5 | 9770-27068 | 9.5 | 70.2 | 5 |
| 5784.75 | PrI | 5.5 | 14505-31787 | 5.5 | 16.2 | - |
| 5786.17 | PrII | 5 | 7438-24716 | 5 | 18.9 | 5 |
| 5791.36 | PrII | 5 | 9379-26641 | 5 | 13.5 | 5 |
| 5792.27 | PrI | 5.5 | 1377-18636 | 4.5 | 13.5 | 11 |
| 5792.95 | PrI | 8.5 | 9770-27027 | 9.5 | 59.3 | 5 |
| 5805.95 | PrI | 5.5 | 11283-28502 | 4.5 | 48.6 | - |
| 5809.35 | PrI | 5.5 | 6714-23923 | 5.5 | 59.3 | - |
| 5811.78 | PrI | 5.5 | 1376-18578 | 4.5 | - | - |
| 5813.55 | PrII | 7 | 11005-28202 | 8 | 35.1 | 5 |
| 5815.17 | PrII | 6 | 8465-25657 | 6 | 29.7 | 11 |
| 5820.76 | PrI | 4.5 | 8250-25425 | 3.5 | 48.6 | 5 |
| 5821.36 | PrI | 4.5 | 8250-25423 | 3.5 | 43.2 | 5 |
| 5822.59 | PrII | | - | | 35.1 | 5 |
| 5830.94 | PrII | 6 | 8465-25610 | 6 | 56.7 | 5 |
| 5831.45 | PrI | 6.5 | 8733-25877 | 7.5 | 13.5 | 13 |
| 5835.13 | PrI | 5.5 | 4866-21999 | 6.5 | 29.7 | 5 |
| 5844.65 | PrII | 7 | 5079-22184 | 7 | 13.5 | 5 |
| 5847.13 | PrII | 7 | 10030-27128 | | 24.3 | 5 |
| 5850.12 | PrI | 7.5 | 4381-21470 | 6.5 | 21.6 | - |
| 5850.64 | PrII | 6 | 3403-20491 | 7 | 8.1 | 5 |

| | | | | | | |
|---|---|---|---|---|---|---|
| 5854.44 | PrI | | - | | 54.0 | 5 |
| 5856.07 | PrII | | - | | 8.1 | 5 |
| 5856.90 | PrII | 5 | 10535-27604 | 6 | 16.1 | 5 |
| 5858.63 | PrI | 8.5 | 10720-27784 | 8.5 | 35.1 | - |
| 5859.69 | PrII | 5 | 11448-28509 | 6 | 40.5 | 5 |
| 5862.45 | PrI | 5.5 | 6714-23767 | 5.5 | 43.2 | - |
| 5869.96 | PrI | 6.5 | 9684-26715 | 6.5 | 16.2 | - |
| 5871.01 | PrI | 4.5 | 5823-22851 | 5.5 | 51.3 | - |
| 5874.72 | PrI | 7.5 | 4381-21398 | 7.5 | 40.5 | 5 |
| 5875.71 | PrI | 5.5 | 8829-25843 | 6.5 | 54.0 | - |
| 5878.10 | PrI | 7.5 | 9647-26654 | 7.5 | 81.0 | 5 |
| 5879.04 | PrI | 7.5 | 8364-25369 | 8.5 | 70.2 | 11 |
| 5884.72 | PrI | 4.5 | 5823-22811 | 5.5 | 105.4 | 5 |
| 5886.16 | PrI | 4.5 | 11184-28168 | 5.5 | 37.8 | - |
| 5891.04 | PrI | 6.5 | 9684-26654 | 7.5 | 51.3 | - |
| 5892.23 | PrII | 8 | 11611-28578 | 7 | 16.2 | 5 |
| 5894.22 | PrII | | - | | 64.8 | 5 |
| 5903.11 | PrII | | - | | 24.3 | 5 |
| 5908.67 | PrII | | - | | 21.6 | 5 |
| 5915.31 | PrI | 5.5 | 6893-23793 | 6.5 | 127.0 | 11 |
| 5915.97 | PrI | 6.5 | 7630-24529 | 7.5 | 127.0 | 11 |
| 5919.78 | PrI | 4.5 | 0000-16887 | 4.5 | 54.0 | 11 |
| 5920.76 | PrI | 6.5 | 6603-23488 | 7.5 | 229.8 | 11 |
| 5925.13 | PrI | 7.5 | 8364-25236 | 6.5 | 5.4 | - |
| 5929.49 | PrI | 9.5 | 12945-29806 | 10.5 | 48.6 | 5 |
| 5930.66 | PrII | 4 | 10117-26973 | 5 | 18.7 | 5 |
| 5931.51 | PrI | 6.5 | 8733-6.5 | | | 11 |
| 5936.33 | PrI | 4.5 | 10936-27777 | 5.5 | 64.9 | 5 |
| 5939.90 | PrII | 7 | 10030-26861 | 7 | 67.6 | 5 |
| 5941.65 | PrI | 7.5 | 8364-25189 | 8.5 | 108.1 | 11 |
| 5949.76 | PrI | 8.5 | 10720-27523 | 8.5 | 86.4 | 5 |
| 5951.76 | PrII | 2 | 8966-25763 | 3 | 8.1 | 5 |
| 5954.79 | PrI | 4.5 | 11713-28502 | 4.5 | 13.5 | - |
| 5956.25 | PrI | 5.5 | 6893-23677 | 6.5 | 91.9 | 11 |
| 5956.75 | PrI | 8.5 | 9770-26553 | 7.5 | 13.5 | 11 |
| 5959.25 | PrI | 7.5 | 10669-27445 | 6.5 | 78.3 | 5 |

| 5959.94 | PrI | 5.5 | 6313-23087 | 4.5 | 29.7 | - |
|---|---|---|---|---|---|---|
| 5962.18 | PrI | 5.5 | 1376-18144 | 5.5 | 218.9 | 11 |
| 5963.00 | PrI | 6.5 | 8733-25499 | 6.5 | 72.9 | 11 |
| 5963.74 | PrI | 7.5 | 9647-26410 | 7.5 | 16.2 | - |
| 5966.10 | PrI | 4.5 | 8250-25007 | 5.5 | 24.3 | - |
| 5967.82 | PrII | 6 | 9647-26398 | 6 | 91.9 | 5 |
| 5970.43 | PrI | 3.5 | 6535-23280 | 4.5 | 45.9 | - |
| 5976.95 | PrI | 5.5 | 1376-18103 | 5.5 | 108.1 | 5 |
| 5978.88 | PrI | 6.5 | 8734-25454 | 6.5 | 97.3 | 5 |
| 5979.67 | PrI | 5.5 | 6893-23611 | 5.5 | 27.0 | - |
| 5981.19 | PrII | 7 | 11794-28509 | 6 | 29.7 | 5 |
| 5984.24 | PrI | 7.5 | 9647-26352 | 6.5 | 48.6 | - |
| 5986.14 | PrI | 9.5 | 11913-28613 | 9.5 | 140.5 | 5 |
| 5987.14 | PrI | 4.5 | 10936-27634 | 4.5 | 62.1 | 5 |
| 5994.89 | PrI | 3.5 | 8013-24689 | 4.5 | 81.0 | 5 |
| 5996.06 | PrI | 6.5 | 9684-26357 | 5.5 | 102.7 | 11 |
| 6000.26 | PrI | 5.5 | 6313-22974 | 6.5 | 32.4 | - |
| 6002.44 | PrII | 4 | 8100-24755 | 4 | 35.5 | 5 |
| 6006.33 | PrII | 8 | 13374-30018 | 7 | 24.3 | 5 |
| 6008.54 | PrI | 5.5 | 8835-25474 | 4.5 | 113.5 | 11 |
| 6010.25 | PrI | 5.5 | 9268-25902 | 6.5 | 18.9 | - |
| 6016.48 | PrII | 4 | 8100-24716 | 5 | 16.2 | 5 |
| 6017.80 | PrII | 2 | 8966-25578 | 3 | 89.2 | 5 |
| 6019.85 | PrI | 10.5 | 13198-29805 | 10.5 | 91.8 | 5 |
| 6025.72 | PrII | 8 | 11611-28202 | 8 | 32.4 | 5 |
| 6031.58 | PrI | 5.5 | 9268-25843 | 6.5 | 35.1 | - |
| 6037.62 | PrI | 6.5 | 10266-26824 | 5.5 | 75.6 | - |
| 6042.87 | PrII | 6 | 10163-26707 | 5 | 78.3 | 5 |
| 6045.04 | PrI | 5.5 | 8829-25367 | 5.5 | 24.3 | - |
| 6046.66 | PrII | 3 | 9045-25578 | 3 | 181.0 | 5 |
| 6049.26 | PrI | 6.5 | 7630-24156 | 7.5 | 129.7 | 5 |
| 6050.04 | PrII | 4 | 10117-26641 | 5 | 13.5 | 5 |
| 6050.88 | PrI | 5.5 | 8835-25357 | 6.5 | 78.3 | 5 |
| 6055.13 | PrI | 5.5 | 8080-24591 | 4.5 | 100.0 | 5 |
| 6067.27 | PrII | 6 | 10163-26641 | 5 | 8.1 | 5 |
| 6068.29 | PrI | 5.5 | 8080-24555 | 6.5 | 91.8 | - |

| | | | | | | |
|---|---|---|---|---|---|---|
| 6083.09 | PrI | 5.5 | 4866-21301 | 5.5 | 59.4 | - |
| 6085.81 | PrI | | 8250-24677 | | 10.8 | 5 |
| 6086.16 | PrII | 5 | 10536-26962 | 6 | 32.4 | 5 |
| 6087.52 | PrII | 3 | 9045-25467 | 2 | 37.8 | 5 |
| 6089.51 | PrI | 7.5 | 4381-20798 | 6.5 | 24.3 | - |
| 6090.38 | PrII | 7 | 10030-26445 | 7 | 81.0 | 5 |
| 6093.09 | PrII | 7 | 11794-28202 | 8 | 21.6 | 5 |
| 6105.91 | PrI | 5.5 | 6714-23087 | 4.5 | 81.0 | - |
| 6106.72 | PrII | 4 | 9129-25500 | 5 | 8.1 | 5 |
| 6109.10 | PrI | 5.5 | 4866-21231 | 6.5 | 159.4 | 5 |
| 6111.94 | PrI | 5.5 | 6313-22670 | 6.5 | 62.1 | - |
| 6114.38 | PrII | 8 | 13374-29724 | 8 | 37.8 | 5 |
| 6122.15 | PrI | 7.5 | 10668-26998 | 7.5 | 40.5 | 5 |
| 6130.27 | PrI | 6.5 | 11746-28054 | 5.5 | 48.6 | - |
| 6139.42 | PrI | 5.5 | 10431-26715 | 6.5 | 21.6 | - |
| 6141.51 | PrII | 5 | 9379-25657 | 6 | 54.1 | 5 |
| 6148.23 | PrI | 5.5 | 6714-22974 | 6.5 | 56.8 | 5 |
| 6157.82 | PrII | 6 | 10163-26398 | 6 | 16.2 | 5 |
| 6159.10 | PrII | 5 | 9379-25610 | 6 | 43.2 | 5 |
| 6173.30 | PrI | 4.5 | 6892-23087 | 5.5 | 21.6 | - |
| 6177.64 | PrI | 6.5 | 6603-22786 | 6.5 | 48.6 | - |
| 6182.34 | PrII | 8 | 11611-27782 | 8 | 48.6 | 5 |
| 6187.96 | PrI | 6.5 | 9684-25840 | 6.5 | 35.1 | 5 |
| 6197.45 | PrII | 6 | 10730-26861 | 7 | 24.3 | 5 |
| 6204.17 | PrI | 5.5 | 9268-25382 | 6.5 | 24.3 | - |
| 6210.59 | PrI | 5.5 | 6714-22811 | 5.5 | 45.9 | 5 |
| 6218.06 | PrI | | - | | 24.3 | 5 |
| 6229.75 | PrI | 5.5 | 11944-27991 | 6.5 | 32.4 | - |
| 6236.99 | PrI | 5.5 | 1376-17405 | 5.5 | 8.1 | 5 |
| 6241.05 | PrI | 9.5 | 12945-28964 | 10.5 | 116.2 | - |
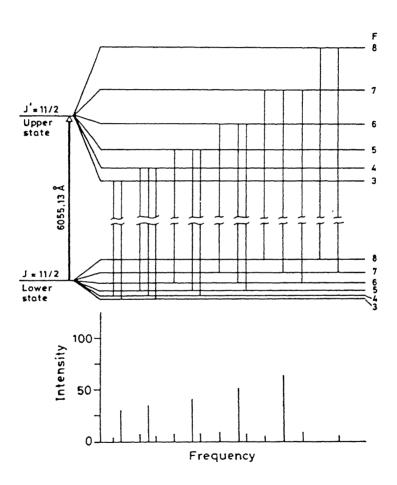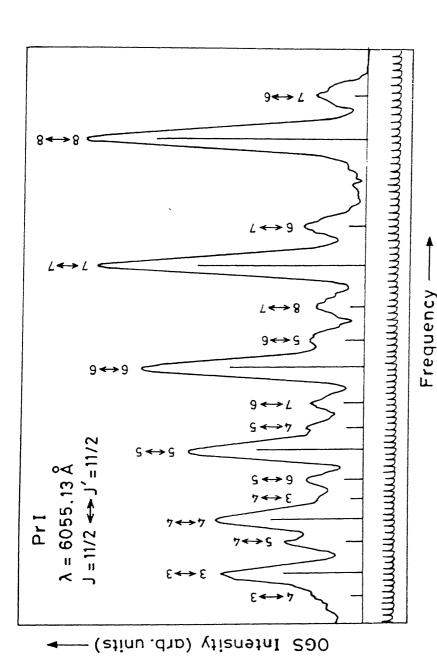
Fig. VI.2  The hfs level scheme of  PrI  line  λ=6055.13Å.  Thereotical
intensity ratios for the hfs components are given at the bottom of the
figure.

Fig.VI.3 Recorded hfs spectrum of PrI line λ=6055.13A. Vertical bars indicate the positions of hyperfine components and their length proportional to the theoretically expected relative intesities. The components are identified by F quantum numbers from lower-state to upper-state.
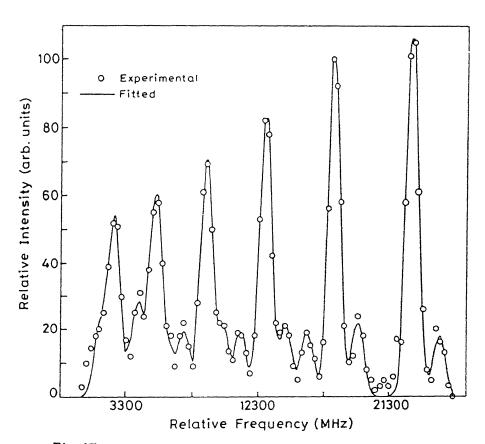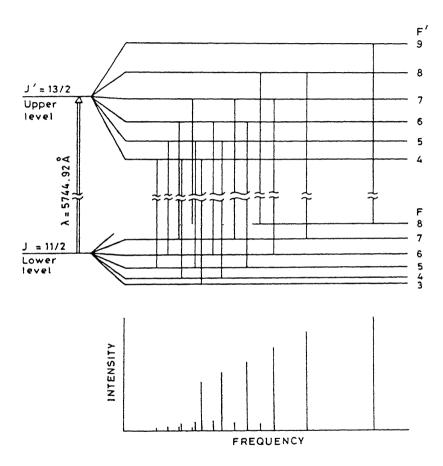
Fig. VI.4   Fitted hfs spectrum of PrI line λ=6055.13Å.

Fig. VI.5   The hfs level scheme of PrI line λ=5744.92Å. Thereotical intensity ratios for the hfs components are given at the bottom of the figure.

Fig. VI.6(b) Fitted hfs spectrum of PrI line

λ=5744.92Å.
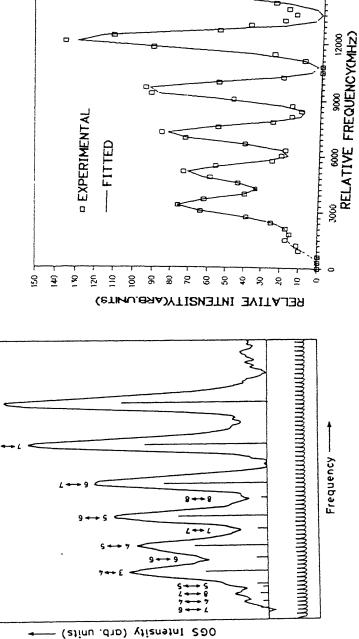


Fig.VI.6(a) Recorded hfs spectrum of PrI line

λ=5744.92Å.
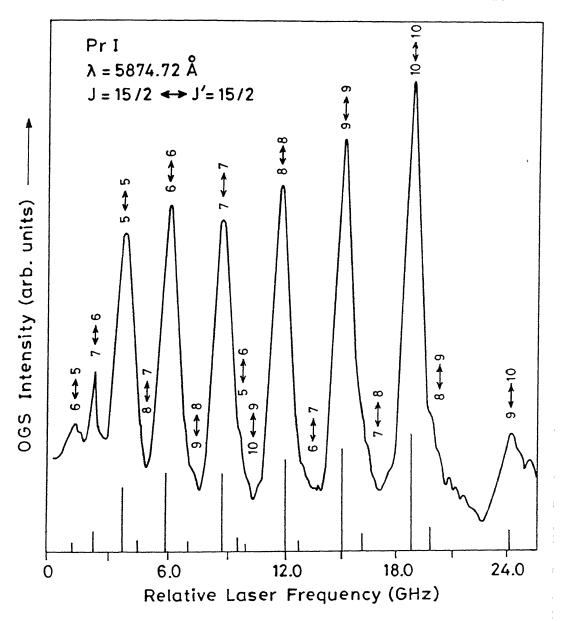
Fig. VI.7   Recorded hfs spectrum of PrI line λ=5874.72Å.
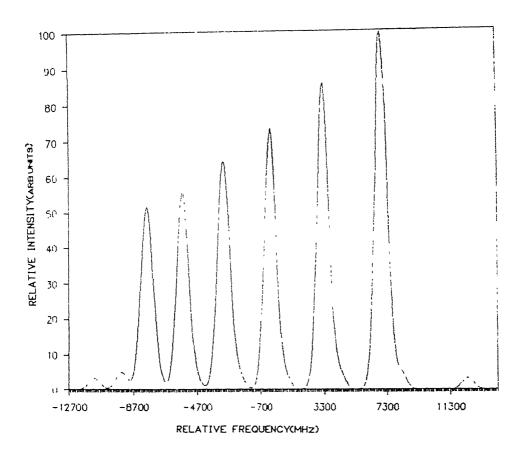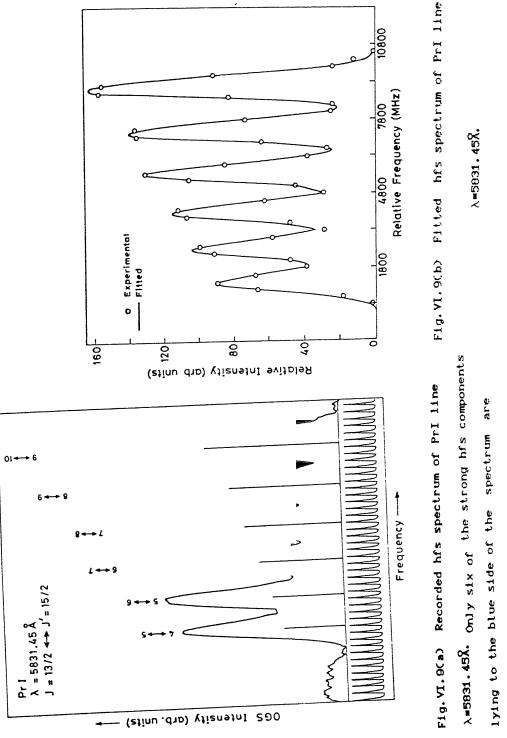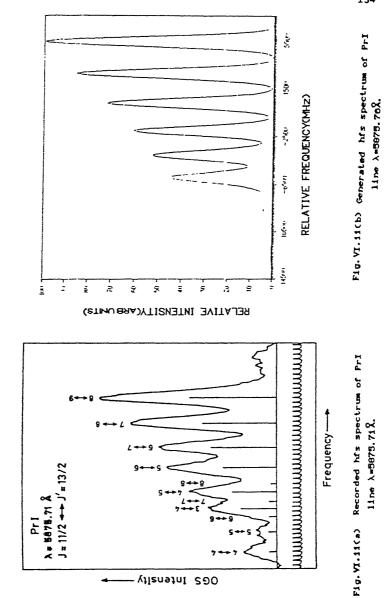
Fig. VI.8   Generated hfs spectrum of PrI line λ=5874.72Å using   the
fitted hfs constants and the theoretical intensities.

Fig.VI.9(b) Fitted hfs spectrum of PrI line

λ=5831.45Å.



Fig.VI.9(a) Recorded hfs spectrum of PrI line

λ=5831.45Å. Only six of the strong hfs components

lying to the blue side of the spectrum are

given in the figure.

Fig.VI.11(b) Generated hfs spectrum of PrI
line λ=5875.76Å.

Fig.VI.11(a) Recorded hfs spectrum of PrI
line λ=5875.71Å.

134

hfs constants were estimated by measuring the spacing between various diagonal hfs components and using them in Casimir formula. The fitting becomes difficult in Pr as the intensities of the individual hfs components are generally not measurable directly. However the intensities of the unresolved hfs components are estimated by normalising the classical intensities to the observed intensity of a well resolved hfs component in the spectrum. As it is discussed in chapter IV the intensities of the individual components of a hyperfine spectrum in OGS often deviate from the expected intensities due to the saturation effects. Therefore the power of the excitation laser was always maintained at lower level($\leq$45mW) while recording the hfs spectra. The recorded and fitted hfs spectra of PrI line $\lambda$=6055.13$\overset{o}{A}$ are shown in Fig.IV.3 and Fig.IV.4 respectively. In this spectrum 14 of the 16 hfs components are well resolved and hence the fitting of it was not very difficult. The hfs constants for nine high lying states belonging to two mixed configurations $4f^2 5d^2 6p$ and $4f^3 5d6p$ were determined for the first time. The hyperfine coupling constants of all the states studied are tabulated in Table VI.2. Our LOGS data are in good agreement, within our experimental accuracy, with the data reported by others who used other experimental methods. The uncertainities in the measurements were estimated in the same way as detailed in chapter IV of the thesis. Since the quadrupole interaction in $^{141}$Pr is very small the fitted B parameters are not that accurate.

Table VI.2  Hyperfine coupling constants of $^{141}$PrI determined by LOGS. The values in parentheses are uncertainities in the last recorded digits. The uncertainities in the measurement of the B-parameters are generally very large.

| Excitation energy ($cm^{-1}$) | J Parity | hfs constants(MHz) | | | | Ref. |
|---|---|---|---|---|---|---|
| | | This work(LOGS) | | Other work | | |
| | | A | B | A | B | |
| 1376.60 | 11/2$^-$ | 729.8(50) | -17 | 730.393 | -11.877 | 11 |
| 4381.10 | 15/2$^-$ | 541.2(50) | -7 | 541.575 | -14.558 | 11 |
| 4866.54 | 11/2$^+$ | 870.8(40) | -43 | 867.997 | -50.319 | 11 |
| 6603.60 | 13/2$^+$ | 754.3(60) | -32 | 755.456 | -48.633 | 11 |
| 6714.22 | 11/2$^+$ | 476.9(60) | -29 | 474.692 | -29.33 | 11 |
| 8080.49 | 11/2$^-$ | 238.5(40) | -19 | 238.352 | -22.961 | 11 |
| 8250.22 | 9/2$^-$ | 214.2(40) | -8 | 213.531 | -4.136 | 11 |
| 8733.45 | 13/2$^-$ | 851.8(60) | -22 | 854.297 | -31.807 | 11 |
| 8829.09 | 11/2$^+$ | 751.5(90) | 8 | 780(36) | - | 10 |
| 8835.42 | 11/2$^-$ | 947.2(70) | -27 | 949.091 | -13.721 | 11 |
| 9646.90 | 15/2$^-$ | 904.3(60) | -16 | 907.515 | -23.132 | 11 |
| 9684.24 | 13/2$^-$ | 988.7(90) | 13 | 991.907 | -7.246 | 11 |
| 9770.33 | 17/2$^+$ | 905.4(40) | -27 | 905.498 | -40.819 | 11 |
| 14505.11 | 11/2$^+$ | 772.0(120) | - | - | - | - |
| 18578.24 | 9/2$^+$ | 611.3(80) | 13 | 608.8 | - | 11 |
| 21398.47 | 15/2$^+$ | 912.7(60) | - | 913.0 | - | 11 |
| 21999.38 | 13/2$^-$ | 975.8(110) | -6 | 976.1 | - | 11 |
| 23923.09 | 11/2$^-$ | 723.2(90) | - | - | - | - |
| 24022.44 | 11/2$^-$ | 317.5(110) | - | - | - | - |

| | | | | | | |
|---|---|---|---|---|---|---|
| 24053.70 | $13/2^-$ | 455.1(80) | −12 | − | − | − |
| 24116.07 | $13/2^-$ | 740.4(60) | −12 | − | − | − |
| 25423.58 | $7/2^+$ | 1201.2(40) | − | 1198.0 | − | 11 |
| 24590.84 | $11/2^+$ | 913.4(80) | − | 914.7 | − | 11 |
| 25843.56 | $13/2^-$ | 846.7(100) | 53 | − | − | − |
| 25877.09 | $15/2^+$ | 945.1(90) | 46 | − | − | − |
| 26654.48 | $15/2^-$ | 530.2(70) | − | 534.5 | − | 11 |
| 26715.43 | $13/2^+$ | 518.0(100) | − | − | − | − |
| 27068.73 | $19/2^-$ | 579.7(70) | −26 | 579.5 | − | 11 |
| 27275.70 | $17/2^-$ | 564.2(90) | −14 | − | − | − |
| 31787.07 | $11/2^-$ | 282.9(90) | −64 | − | − | − |

## VI.5  CONCLUSIONS

LOGS is a useful technique for studying both the fine and the hyperfine specrta of the high-lying configurations of PrI including of the mixed configurations $4f^2 5d^2 6p$ and $4f^3 5d6p$ using hollow cathode discharge lamps. The present results on several new transitions of PrI and their estimate of the intensities are very useful for understanding the high-lying mixed configurations in PrI. The hyperfine structure data are not only valuable for the classification of the levels but also useful for evaluating the radial parameters of different electrons in Pr. However for the unambiguous classification of the highly dense spectrum of Pr, it would be better to employ a Doppler-free method to study the hyperfine structure of the spectral lines.

# REFERENCES

1. A.S.King, Astrophys.J.68, 194(1928)

2. R.Zalubas and M.Wilson, J.Research Natl. Bur. Stand.(U.S)69A,59(1965)

3. R.Zalubas and B.R.Borchardt, J.Opt.Soc.Am.63,102(1973)

4. J.Blaise, J.Verges, J.-F.Wyart and R.Zalubas, J.Opt.Soc.Am.63,1315(1973).

5. Tables of Spectral Line Intensities, Arranged by Elements. W.F.Meggers, C.H.Corliss, and B.F.Scribner, eds. (U.S.Government Printing Office, Washington,1975)

6. Atomic Energy Levels, The Rare Earth Elements, W.C.Martin, R.Zalubas, and L.Hagan,eds.(U.S.Governament Printing Office, Washington,1978)

7. H.Lew, Phys.Rev.91,619(1953)

8. K.D.Boklen, T.Bossert, W.Foerster, H.H.Fuchs, and G.Nachtsheim, Z.Phys.A274, 195(1975)

9. N.F.Ramsey, Phys.Rev.76, 996(1949)

10. A.Ginibre, Phys.Scr.23, 260(1981)

11. W.J.Childs and L.S.Goodman, Phys.Rev. A24, 1342(1981)

12. M.N.Reddy and G.N.Rao, Physica C150, 457(1988)

13. J.Blaise and A.Ginibre (private communication)

A 108479

PHY — 1989 — D — RED — FIN